THE ASTRONOMICAL JOURNAL VOLUME 114, NUMBER 2 AUGUST 1997

THE SPECTRAL ENERGY DISTRIBUTION OF NORMAL, STARBURST, AND ACTIVE GALAXIES

HENRIQUE R. SCHMITT[1]

Departamento de Astronomia, IF-UFRGS, CP 15051, CEP91501-970, Porto Alegre, RS, Brazil and Space Telescope Science Institute, 3700 San Martin Drive, Baltimore, Maryland 21218
Electronic mail: schmitt@if1.if.ufrgs.br

ANNE L. KINNEY

Space Telescope Science Institute, 3700 San Martin Drive, Baltimore, Maryland 21218 and Department of Physics and Astronomy, Johns Hopkins University, Baltimore, Maryland 21218
Electronic mail: kinney@stsci.edu

DANIELA CALZETTI

Space Telescope Science Institute, 3700 San Martin Drive, Baltimore, Maryland 21218
Electronic mail: calzetti@stsci.edu

THAISA STORCHI BERGMANN

Departamento de Astronomia, IF-UFRGS, CP 15051, CEP91501-970, Porto Alegre, RS, Brazil
Electronic mail: thaisa@if1.if.ufrgs.br

Received 1997 February 6; revised 1997 May 12

ABSTRACT

We present the results of an extensive literature search of multiwavelength data for a sample of 59 galaxies, consisting of 26 Starbursts, 15 Seyfert 2's, 5 LINER's, 6 normal spirals, and 7 normal elliptical galaxies. The data include soft X-ray fluxes, ultraviolet, and optical spectra, near-, mid/far-infrared photometry, and radio measurements, selected to match as closely as possible the *IUE* aperture ($10'' \times 20''$). The galaxies are separated into 6 groups with similar characteristics, namely, ellipticals, spirals, LINER's, Seyfert 2's, starbursts of low and high reddening, for which we create average spectral energy distributions (SEDs). The individual groups SEDs are normalized to the λ7000 Å flux and compared, looking for similarities and differences among them. We find that the SEDs of normal spirals and ellipticals are very similar over the entire energy range, and fainter than those of all other groups. LINER's SEDs are similar to those of Seyfert 2's and Starbursts only in the visual to near-IR waveband, being fainter in the remaining wavebands. Seyfert 2's are similar to Starbursts in the radio to near-IR waveband, fainter in the visual to ultraviolet, but stronger in the X-rays. Low and high reddening Starbursts are similar along the entire SED, differing in the ultraviolet, where Low reddening Starbursts are stronger, and in the mid/far-IR where they are fainter. We have also collected multiwavelength data for 4 H II regions, a thermal supernova remnant, and a non-thermal supernova remnant (SNR), which are compared with the Starburst SEDs. The H II regions and thermal SNRs have similar SEDs, differing only in the X-ray and far infrared. The non-thermal SNR SED is a flat continuum, different from all the other SEDs. Comparing the SEDs of Starbursts and H II regions we find that they are similar in the mid/far-IR parts of the spectrum, but H II regions are fainter in the radio and X-rays. Starbursts are also stronger than H II regions in the visual and near-IR parts of the spectrum, due to the contribution from old stars to starbursts. The bolometric fluxes of the different types of galaxies are calculated integrating their SEDs. These values are compared with individual waveband flux densities, in order to determine the wavebands which contribute most to the bolometric flux. In Seyfert 2's, LINER's, and starbursts, the mid/far-IR emission are the most important contributers to the bolometric flux, while in normal spirals and ellipticals this flux is dominated by the near-IR and visual wavebands. Linear regressions were performed between the bolometric and individual band fluxes for each kind of galaxy. These fits can be used in the calculation of the bolometric flux for other objects of similar activity type, but with reduced waveband information. © *1997 American Astronomical Society.* [S0004-6256(97)02508-9]

1. INTRODUCTION

With the present availability of large databases, including satellite observations at wavebands that cannot be observed from the ground, like X-rays, ultraviolet, mid/far-IR, it is possible to construct spectral energy distributions (SEDs) of galaxies over 10 decades of frequency. The study of the continuum emission of galaxies over such a broad range of frequencies is important for a good determination of the bolometric luminosity of these objects. Also, the SEDs can be

[1]CNPq Fellow.

 0004-6256/97/114(2)/592/21/$10.00

used to study the energy output at different wavebands, as well as a means to distinguish galaxies of different activity classes.

Previous works, like those of Edelson & Malkan (1986) and Sanders *et al.* (1989) investigated the SEDs of AGNs. Edelson & Malkan (1986) analyzed a small group of Seyfert 1's, Seyfert 2's, and quasars, but did not include radio and X-ray fluxes in their SEDs, while Sanders *et al.* (1989) presented radio to X-ray SEDs for a sample of radio loud and radio quiet quasars.

While the SEDs of high luminosity AGNs have been relatively well studied, little has been done on the SEDs of starbursts, Seyfert 2's, LINER's, and normal galaxies. Mas-Hesse *et al.* (1994, 1995) have presented a radio to X-ray multiwavelength analysis of Seyfert 1's, Seyfert 2's, starbursts, and quasars, but with relatively sparse data points to cover the frequency range. They found that these objects can be divided into two major groups, those objects where the far-infrared emission dominates the SED (Seyfert 2's and starbursts), and those objects where the UV and X-ray have fluxes comparable to the far-infrared (QSOs and Seyfert 1's). They also point out that Seyfert 2's and starbursts have similar SEDs, but Seyfert 2's are brighter in the X-rays.

Another multiwavelength analysis of starbursts, Seyferts, LINER's, quasars, and normal galaxies was made by Spinoglio *et al.* (1995). They do not use radio and X-ray fluxes and only include a small number of wavebands. Spinoglio *et al.* (1995) also apply a correction to include the flux of the entire galaxy in their analysis, which is uncertain. Their results show that the nonstellar radiation at 2–3 μm correlates with the *IRAS* colors, which produces a sequence of colors, that runs from normal galaxies to Seyfert 2's, Seyfert 1's, and quasars. Starbursts fall outside this sequence, because they have an excess of 60 μm emission. In contrast to Mas-Hesse *et al.* (1995), Spinoglio *et al.* (1995) found that in the mid/far infrared Seyfert 2's are more similar to Seyfert 1's than to the starbursts, which they attribute to the fact that Seyferts are heated by a single source, while Starbursts have an extended heating region.

In this paper we present the spectral energy distribution from radio ($\nu \approx 10^8$ Hz) to soft X-rays ($\nu \approx 10^{18}$ Hz) of a sample of galaxies including starbursts, Seyfert 2's, LINER's, normal spirals, and ellipticals. While the data were selected in order to match as closely as possible the *IUE* aperture ($10'' \times 20''$), the match is indeed not very good, and is the main challenge in assembling and interpreting such a data set. The galaxies were divided in 6 groups according to activity class and, in the case of quiescent galaxies, according to morphology, for which we create average SEDs. These average SEDs are compared to verify whether we can use the SEDs to separate different activity classes. We also present the SEDs of H II regions, a thermal SNR and a nonthermal SNR, which are compared to starburst SEDs.

In Sec. 2 we describe our sample and in Sec. 3 we discuss the data and aperture effects. The SEDs of the individual groups are described in Sec. 4 and compared in Sec. 5. In Sec. 6 we describe the H II regions and supernova remnants SEDs and compare them with starbursts SEDs. A statistical comparison between the SEDs of galaxies with different activity classes is given in Sec. 7. The bolometric luminosities are discussed in Sec. 8, while in Sec. 9 we give the summary.

2. THE SAMPLE

The galaxies were selected from the catalog of ultraviolet *IUE* spectra of Kinney *et al.* (1993) and from Kinney *et al.* (1996). We include only those objects for which we have ground based spectra, observed with apertures matching that of *IUE* (Storchi-Bergmann *et al.* 1995; McQuade *et al.* 1995; Kinney *et al.* 1996).

The sample is composed of 59 objects, with 26 star-forming galaxies, 15 Seyfert 2's, 5 LINER's, 6 normal spirals, 6 normal ellipticals, and 1 bulge of a spiral (NGC 224, which is treated as an elliptical). Their names, morphological types, activity classes, radii and velocities relative to the local group of galaxies are given in Table 1. For objects with composite activity class we assume that the first class listed in the reference is dominant.

3. THE DATA AND APERTURE EFFECTS

We searched the literature for X-ray, infrared and radio data of the sample galaxies, selecting, when possible, data observed with apertures close to that of the *IUE* satellite ($10'' \times 20''$). Note that although the apertures do not match very well, a comparison between bolometric fluxes and galaxy diameters (Sec. 8), shows that these quantities are relatively independent. Thus the aperture effects do not generally dominate the data.

The UV and optical data ($14.5 \leqslant \log \nu \leqslant 15.5$) were obtained from Table 4 of McQuade *et al.* (1995) and Table 4 of Storchi-Bergmann *et al.* (1995). The UV is composed of *IUE* spectra in the wavelength range 1100–3200 Å, while the optical comes from ground based spectra in the range 3200–10000 Å observed with matched apertures. Details of the observations and reductions are given in the above papers. Notice that instead of using the spectra, we use only the continuum fluxes measured on selected points, because we are interested only on the continuum energy distribution and not on individual spectral features. We give in Table 2 the UV and optical continuum fluxes for 8 galaxies of the sample, also observed by the authors, but whose data were not previously published.

In Table 3 we show the radio data ($\log \nu < 10$), available in the literature, for the objects in Table 1. Since the galaxies were not observed exactly at the same wavelengths we indicate in the table header the approximate wavelengths. The information for each entry is divided in three lines; on the first line we give the flux (in units of mJy), on the second line we give the actual frequency of the observation (in units of GHz), and on the third line the aperture through which it was observed. On the last column we give the references from which each entry of the table was obtained, ordered from left to right, according to the numbers listed in Table 4. The apertures for the radio data vary from 3″ to apertures of the order of arcminutes, containing the entire galaxy. This spread in apertures introduces a large spread in the fluxes, with the smaller apertures including only nuclear emission

TABLE 1. Sample properties.

Name	Morphological Type	Activity Class	Radius	V (km s^{-1})
NGC210	Sb		2′30″	1678
NGC221	E2		4′42″	−28
NGC224	Sb		80′00″	−121
IC1586		BCG	9″	5963
NGC262	S0	Sy2	33″	4669
HARO15	I	BCG	27″	6447
MRK357	Pair?	SB nuc.	6″	15973
NGC598	Scd		35′24″	−46
IC214	pec.,2-nuc.	SB nuc.	24″	9101
NGC1023	SB0		4′33″	749
NGC1068	Sb	Sy2	3′33″	1144
NGC1097	SBbc	Hs+Lin	4′39″	1193
NGC1140	Irr. Am.	BCG	51″	1479
NGC1313	SBdm	HII	4′33″	292
NGC1316	E/S0		5′15″	1674
NGC1399	E1 pec		3′27″	1323
NGC1404	E2		1′39″	1805
NGC1433	SBab		3′15″	920
NGC1553	S0 pec.		2′15″	612
NGC1672	SAB(a)bc	SB+Sy	3′18″	1155
NGC1667	Sbc	Sy2	48″	4459
NGC3031	Sb	Lin	13′27″	69
NGC3049	SBbc	SB nuc.	1′6″	1372
NGC3081	SBa	Sy2	1′6″	2164
NGC3256	Sb(s)pec	SB nuc.	1′54″	2558
NGC3660	SBbc	Sy1/NELG	1′21″	3529
NGC4385	SBab	SB nuc.	1′6″	2053
NGC4569	SABab	Lin	4′45″	−283
NGC4579	Sab	Lin	2′57″	1470
NGC4594	Sa	Lin	4′21″	969
IC3639	SBb	Sy2	36″	3137
NGC5135	SABb	Sy2	1′18″	3959
MRK66		BCG	12″	6638
NGC5236	SBc	SB nuc.	6′27″	384
NGC5253	Im Am.	SB nuc.	2′30″	271
NGC5506	Sa pec.	Sy2	1′24″	1782
NGC5643	SBc	Sy2	2′18″	1066
MRK477	Comp.	Sy2		11511
NGC5728	Sbb	Sy2	1′33″	2735
UGC9560	Irr. pec.	BCDG	24″	1308
NGC5860	pair of Es	SB nuc.	18″	5520
NGC5996	Sbd	SB nuc.	51″	3389
NGC6052	Cl. Irr.	SB nuc.	30″	4820
NGC6090	Sd pec. pair	SB nuc.	18″	8953
NGC6217	SBbc	SB nuc.	1′30″	1544
NGC6340	Sa		1′42″	1398
NGC6764	SBb	Lin/HII	1′9″	2637
NGC6868	E2		1′45″	2831
NGC7130	Sa pec.	Sy2+SB nuc.	45″	4850
NGC7196	E3		1′15″	2882
NGC7250	S/I	SB nuc?	51″	1380
NGC7496	SBc	Sy2+HII	1′39″	1623
NGC7552	SBbc	SB nuc.	1′42″	1568
NGC7582	SBab	Sy2+SB	2′30″	1551
NGC7590	SAbc	Sy2	1′21″	1569
NGC7673	Cl. Irr.	HII	39″	3581
NGC7714	Sdm pec.	SB nuc.	57″	2925
MRK542	Comp.	HII	6″	7457
NGC7793	SAd	HII	4′39″	228

Notes to TABLE 1

The morphological type, radius and velocities, relative to the local group of galaxies, were obtained from NED. The Activity Class was obtained from Kinney *et al.* (1993), while normal galaxies have no activity class indicated. We will use $H_0 = 75$ km s^{-1} Mpc^{-1} throughout this paper.

and the larger apertures including also extended radio emission and emission from H II regions and SNRs along the galaxy disk, significantly increasing the flux.

Millimeter, near-infrared (1.2–20 μm) and X-ray data are shown in Table 5, in the same format as in Table 3. Millimeter data are rare, being available only for 3 Seyfert 2 galaxies. These data can be considered only as additional information for these galaxies, since we cannot compare them with the other classes of objects. Data in the near-infrared range ($13.5 \leqslant \log \nu \leqslant 14.5$) are available for the majority of the galaxies in our sample, usually with apertures very close to that of *IUE*.

For the X-ray waveband ($\log \nu > 15.5$) we use data from the *Einstein* catalog of Fabbiano *et al.* (1992). We chose to use *Einstein* instead of *ROSAT* data, because it has observations available for a larger number of galaxies, including almost all the galaxies observed with *ROSAT* (the only exception is NGC 3256, for which only *ROSAT* data are available). The aperture in the X-ray is problematic, because it includes the entire galaxy, with both extended emission and sources in the galaxy disk, farther than the 10″ × 20″ central region. In the case of Starbursts and Seyfert 2's, where most of the X-ray flux comes from the nuclear region, the aperture does not affect the results considerably. However, for LINER's and normal galaxies, this assumption is not valid, and their X-ray fluxes may be strongly contaminated by H II regions, supernova remnants and X-ray binaries along the disk of the galaxy.

The X-ray fluxes given in Table 5 are integrated over the entire waveband (0.2–4.0 keV for *Einstein* or 0.1–2.4 keV for *ROSAT*). In order to put these fluxes in the same units as the other wavebands, we assume the X-ray spectrum to be $\propto \nu^{-1}$, and calculate the flux to the central energy of the band (2.1 keV for *Einstein* and 1.25 keV for *ROSAT*). The assumption of a slope of -1 (ν^{-1}) would underestimate the central energy flux by 40% if the true slope was -0.5, or overestimate it by 40% if the true slope was -1.5.

The *IRAS* data ($12.5 \leqslant \log \nu \leqslant 13.5$), in the mid/far-IR (12, 25, 60, and 100 μm), were obtained from NED (NASA Extragalactic Database). Due to the large aperture through which they were obtained, which varies from 0.75′ × 4.5′ at the 12 μm band to 3′ × 5′ at 100 μm, these data are challenging for our analysis. The aperture discrepancy is probably the least problematic for starbursts where the light is concentrated towards the nucleus according to Calzetti *et al.* (1995). Likewise, IR emission from the Seyfert 2 galaxies is probably also dominated by nuclear emission. However, the emission from the LINER's and normal galaxies is likely strongly contaminated by sources throughout the galaxy disk.

4. SPECTRAL ENERGY DISTRIBUTIONS

The sample is divided in six groups: normal ellipticals, normal spirals, Seyfert 2's, LINER's, and high and low reddening starbursts. The division between low and high reddening starbursts is made at $E(B-V) = 0.4$, assuming the values given by Calzetti *et al.* (1994). The low reddening group is composed of the galaxies: HARO 15, MRK 357,

TABLE 2. Continuum fluxes.

Wavelength	NGC 210	NGC 221	NGC 1316	NGC 1399	NGC 1404	NGC 6340	NGC 6868	NGC 7196
1355	0.17	0.28	0.21	1.06	0.22	···	0.05	0.24
1455	0.08	0.22	0.18	0.89	0.15	···	···	0.25
1507	···	0.19	0.22	0.75	0.18	···	···	0.23
1583	0.10	0.26	0.13	0.77	0.12	···	0.14	0.08
2530	0.10	1.91	0.23	0.38	0.13	0.01	···	0.08
2900	0.28	4.49	0.81	0.69	0.43	0.26	···	0.25
3500	0.45	9.86	1.56	1.51	1.84	0.41	0.72	0.60
3740	0.64	10.48	1.99	1.81	2.47	0.55	1.13	0.98
3810	0.56	7.96	1.95	2.68	2.66	0.51	0.95	0.86
4020	0.92	17.14	3.11	4.38	3.89	0.96	1.28	1.07
4510	1.36	26.58	4.67	7.24	6.23	1.42	2.67	2.09
4630	1.45	27.52	4.92	7.12	6.62	1.50	3.15	2.42
5313	1.55	29.57	5.14	8.78	7.19	1.72	3.36	2.48
5870	1.86	31.76	5.63	8.90	7.99	1.82	3.95	2.99
6080	1.82	30.47	5.65	9.46	8.03	1.97	3.84	2.87
7043	1.74	26.02	5.33	8.49	8.14	2.07	4.04	2.90
7525	1.80	···	5.48	9.80	8.48	···	4.22	2.99
8180	1.71	···	5.33	9.70	8.32	···	3.93	2.92
8838	1.76	···	5.52	9.67	8.50	···	4.17	3.03

Notes to TABLE 2

Continuum fluxes are in units of 10^{-14} erg cm^{-2} s^{-1} Å^{-1}.

MRK 542, MRK 66, NGC 1140, NGC 3049, NGC 5236, NGC 5253, NGC 6052, NGC 7250, and UGC 9560; while the high reddening one is composed of: IC 1586, IC 214, NGC 1097, NGC 1313, NGC 1672, NGC 3256, NGC 4385, NGC 5860, NGC 5996, NGC 6090, NGC 6217, NGC 7552, NGC 7673, NGC 7714, and NGC 7793.

The foreground Galactic extinction for the galaxies in our sample is small, and no correction is applied. Also, due to the small redshift of the galaxies, only the data in the wavelength range 1100–10000 Å, corresponding to the *IUE* and ground based spectra, were redshift corrected. No redshift correction was applied to the broad band data. The possible errors introduced by these factors are minimal and will not affect the overall analysis.

The individual SEDs of normal elliptical and spiral galaxies are shown in Fig. 1(a). SEDs of Seyfert 2's and LINER's are shown in Fig. 1(b) and those of the starbursts of low and high reddening are shown in Fig. 1(c). From now on we will refer to the low and high reddening Starbursts as SBL and SBH, respectively. The SEDs are shifted in the figures by arbitrary constants, for clarity. The radio and X-ray upper limits are shown as filled dots. Notice also that we draw a straight line from the radio to the far-IR 100 μm wavebands. This assumption do not represent the real SED in the millimeter region which, according to Antonucci *et al.* (1990), present a dip around 1 mm.

The SEDs were normalized to the flux at λ7000 Å, which corresponds to a normalization to the old stellar population contribution, and are shown in Fig. 2. The average SEDs, obtained from the latter, are shown in Fig. 3 and their values are given in Table 6. Since the upper limits presented values similar to the real detections in the same wavebands, we decided to include them in the averages.

As we can see in the above figures, the elliptical galaxies have similar SEDs in the UV to near-IR range, presenting an old, red stellar population, and the UV turn-up. However, in the mid/far-IR and radio wavebands there is a large difference between individual SEDs. The differences in the mid/far-IR can be attributed to different amounts of dust (Goudfrooij & de Jong 1995), while in the radio, the existence of a radio loud nucleus can influence the SED radio tail significantly. These differences could also be due to the different apertures through which the observations were taken. The X-ray fluxes have some spread, which is due to the large aperture through which they were observed, including the contribution from sources like X-ray binaries and the hot gaseous halo (Fabbiano 1989), which extend for much more than $10'' \times 20''$.

Normal spiral galaxy SEDs, when compared with the SEDs of Elliptical galaxies, have a considerable spread in the UV to near-IR, which is due to the presence of H II regions in the disk, close to the nucleus of some of these galaxies. The X-ray data are available for only two objects, showing vastly different values of slope from optical to X-ray and so will not be used in the rest of the analysis. The mid/far-IR emission, like that emission in the ellipticals, have a large spread, which can be attributed to both aperture and dust effects. In the radio waveband, the SEDs are very similar, with the exception of NGC 598, which is the higher radio emitter. This galaxy has a radius far greater than the other spirals in the sample, implying that the difference is due to aperture effects.

The Seyfert 2 galaxies have similar SEDs in the near-IR to radio wavelengths. However, they have a large spread in the UV range, being as red as a normal galaxy or as blue as a starburst. This increasing blueness can be due to an increasing contribution from the AGN continuum to the spectrum, like in NGC 1068, or to the presence of circumnuclear H II regions, like NGC 7130. Figures 2 and 3 also show that there is a steep drop in the emission from far-IR to the millimeter waveband (log $\nu \approx 11.5$). This drop, which is similar to the one observed in quasars (Sanders *et al.* 1989; Anto-

TABLE 3. Radio data.

Name Freq. (GHz) Apert.	5.2 m 0.0577	3.75 m 0.080	2 m 0.150	92 cm 0.326	72 cm 0.417	45 cm 0.667	35 cm 0.857	20 cm 1.50	12 cm 2.50	9 cm 3.33	6 cm 5.00	3.5 cm 8.57	2.8 cm 10.71	2.0cm 15.00	1.2cm 33.33	Refs.
NGC210								7.2 1.49 48″								12
NGC221								<4 1.415 21″								48
NGC224					220 0.408 3′42″			130 1.415 21″			2460 4.85 3′30″					29, 48, 18
IC1586					<100 0.430 10′											97
NGC262					390 0.430 10′			260 1.49 12′			245 4.85 3′30″					97, 16, 18
HARO15				21.5 0.325 22″				18.5 1.489 5″			1.3 4.76 2′28″		6.6 10.7 1′12″			22, 22, 59, 58
MRK357								3.1 1.465 4.4″			1.7 4.885 4.4″					90, 90
NGC598[a]	7500 0.0575 6′15″	7500 0.0704 5′3″	5600 0.1515 6′54″	5650 0.3264 1′21″		4400 0.6095 1′15″	5400 0.842 15′	3200 1.41 10′24″	2400 2.695 5′12″		1100 4.75 2′24″		550 10.7 1′12″			52, 52, 52, 52, 52, 11, 23, 23, 11, 11
IC214								47.4 1.49 15″	88.0 2.73 4′24″							19, 96
NGC1023								<10 1.415 21″								49
NGC1068[b]	39000 0.0575 7′	24000 0.8 3′42″	17900 0.178 15′	12290 0.318 17′	11700 0.408 2′52″	9430 0.635 30′30″	6820 0.96 20′18″	4991 1.49 60″	3070 2.7 8′		1890 5.0 6′	1480 8.0 60″	1020 10.7 1′18″	680 14.9 59″		51, 89, 78, 20, 44, 106, 106, 19, 107, 55, 92, 74, 34
NGC1097					900 0.408 2′52″			415 1.49 60″	253 2.7 8′		30 5.0 18″					44, 15, 107, 49
NGC1140											12 4.75 2′27″		11 10.7 1′10″			56, 56
NGC1313					201 0.408 2′52″		360 0.843 43″		172 2.7 8′		100 5.0 —					44, 93, 107, 46
NGC1316					249000 0.408 2′52″				93500 2.7 8′		65800 5.0 4′18″					44, 83, 83
NGC1399		20000 0.08 —			1400 0.408 2′52″		920 0.843 56″		445 2.7 8′		191.4 4.885 4″	360 8.4 —				108, 12, 46, 83, 84, 108
NGC1404					<100 0.408 2′52″				<30 2.7 8′		<0.7 4.885 4″					44, 83, 84
NGC1433					<70 0.408 2′52″		60 0.843 43″		<50 2.7 8′							44, 93, 107
NGC1553					<50 0.408 2′52″		10 0.843 43″		83 2.7 8′		52 5.0 4′18″					44, 93, 83, 83
NGC1672					700 0.408 2′52″		350 0.843 46″	450 1.41 —	186 2.7 8′		100 5.0 4′18″					12, 46, 108, 107, 46
NGC1667								3.7 1.5 1″			1.0 5.0 1″					100, 100

TABLE 3. (continued)

Name Freq. (GHz) Apert.	5.2 m 0.0577	3.75 m 0.080	2 m 0.150	92 cm 0.326	72 cm 0.417	45 cm 0.667	35 cm 0.857	20 cm 1.50	12 cm 2.50	9 cm 3.33	6 cm 5.00	3.5 cm 8.57	2.8 cm 10.71	2.0cm 15.00	1.2cm 33.33	Refs.
NGC3031	2400 0.0575 7′							60 1.415 21″	135 2.3 5′35″		93 4.85 3′30″	82 8.3 1′35″				51, 48, 5 42, 5
NGC3049									8 2.38 2′42″							26
NGC3081								2.5 1.5 <1″			0.9 5.0 <1″					100, 100
NGC3256		3000 0.08 —			1450 0.408 2′52″				420 2.7 —		56.2 5.0 6″					108, 44, 108, 30
NGC3660											11 5.0 2′30″					63
NGC4385								5.4 1.465 4.5″	13 2.38 2′42″		2.8 4.885 4.5″					90, 25, 90
NGC4569[c]					454 0.408 2′52″			83.4 1.49 48″	63 2.38 2′42″		31 4.85 3′30″					44, 19, 25, 18
NGC4579					500 0.408 2′52″			103 1.49 54″	95 2.38 2′42″		56 4.85 15″					44, 19, 25, 17
NGC4594					107 0.408 2′52″			102 1.49 54″	108 2.7 8′		118 5.0 0.1″					44, 19, 107, 30
IC3639								77.5 1.5 30″			32.8 4.885 13″					100, 102
NGC5135								163.2 1.5 9″			58.8 5.0 9″					100, 100
MRK66											<18 5.0 2′36″					8
NGC5236	29000 0.0575 7′	36000 0.085 —	589 0.151 4′12″		6200 0.408 2′52″		12800 0.843 1′5″	450 1.5 35″	1170 2.7 8′	1030 3.237 —	170 5.0 35″	220 8.4 —	490 10.63 —			51, 45, 21, 44, 42, 73, 107, 45, 73, 108, 45
NGC5253					128 0.408 2′52″						75 5.0 4′					44,30
NGC5506					415 0.408 3″			322 1.49 18″			160 5.0 3″			44 15 0.15″		101, 19, 99, 99
NGC5643					600 0.408 2′52″			41 1.5 28″	138 2.7 8′		20 5.0 28″					44, 71, 107, 71
MRK477								58.3 1.415 6″			25 5.0 1.5″					69, 98
NGC5728					138 0.408 2′52″			44 1.5 20″	51 2.7 8′		12 5.0 20″					44, 87, 107, 87
UGC9560				11.2 0.327 1′12″		6.5 0.609 38.6″		4.3 1.5 6″			3.4 4.76 1′47″		2.7 10.7 2′27″			88, 88, 109, 59, 88
NGC5860									360 2.7 5′6″							62
NGC5996									50 2.73 4′24″		16 5.0 4′18″					96, 107
NGC6052[d]				244 0.325 22″	770 0.430 10′			94 1.49 18″	59 2.38 2′42″		42.4 4.76 1′12″		22 10.7 1′12″		14 25 1′12″	22, 47, 59, 25, 58, 58, 47

TABLE 3. (continued)

Name Freq. (GHz) Apert.	5.2 m 0.0577	3.75 m 0.080	2 m 0.150	92 cm 0.326	72 cm 0.417	45 cm 0.667	35 cm 0.857	20 cm 1.50	12 cm 2.50	9 cm 3.33	6 cm 5.00	3.5 cm 8.57	2.8 cm 10.71	2.0cm 15.00	1.2cm 33.33	Refs.
NGC6090			245 0.151 4′12″					46.4 1.49 15″			19.2 5.0 8″			6 15.0 8″		21, 19, 6, 6
NGC6217				126.5 0.327 55″				33.1 1.5 6.6″			10.1 5.0 6.7″					72, 103, 103
NGC6340								<1.5 1.49 60″								15
NGC6764											46 5.0 25″		10 10.7 3′			7, 53
NGC6868							100 0.843 43″		112 2.7 8′		124 5.0 4′18″					93, 107, 107
NGC7130											70.1 4.885 22″					102
NGC7196									<20 2.7 8′		<10 5.0 4′18″					83, 83
NGC7250							<330 0.968 3′20″			36 3.66 3′20″						85, 85
NGC7496								36.3 1.49 60″	50 2.7 4′18″							15, 107
NGC7552					600 0.408 2′52″			276 1.49 60″	157 2.7 4′18″		28 5.0 6″					44, 15, 107, 30
NGC7582			580 0.408 2′36″			166 1.5 13″	193 2.7 8′		69 5.0 13″							104, 71, 107, 71
NGC7590									76 2.7 4′18″		70 5.0 6″					107, 30
NGC7673								33.9 1.49 15″	30 2.38 2′42″				10.3 10.7 1′12″			19, 25, 47
NGC7714					530 0.430 9′18″		310 0.835 9′42″	52.9 1.49 18″	123 2.73 4′24″		15 5.0 2.8″		<10 10.7 3′			53, 53, 19, 96, 13, 53
MRK542									43 2.38 2′42″							25
NGC7793					107 0.408 2′52″			103 1.49 60″	<50 2.7 8′							44, 15, 107

The fluxes listed in this table are given in mJY, and the references are identified in Table 4. The following galaxies also have some more radio data:

[a]NGC 598: 0.0214 GHz=7000 mJy (16′54″) (Ref. 52); 0.0256 GHz=12000 mJy (14′33″) (Ref. 52); 0.0309 GHz=9000 mJy (12′5″) (Ref. 52); 1.72 GHz =2700 mJy (7′42″) (Ref. 11).

[b]NGC 1068: 0.102 GHz=24000 mJy (60′) (Ref. 3); 0.75 GHz=7600 mJy (18′30″) (Ref. 64).

[c]NGC 4569: 2.7 GHz=89 mJy (8′) (Ref. 107).

[d]NGC 6052: 22.8 GHz=11.1 mJy (42″) (Ref. 58).

nucci *et al.* 1990), represents the end of the thermal emission from radiation reprocessed by the circumnuclear torus and maybe H II regions in the galaxy disk, and the beginning of the non-thermal, synchrotron radio emission.

The LINER SEDs are similar in the radio and visual part of the spectrum, but have some spread in mid/far-IR and UV wavebands. The mid/far-IR spread can be explained using the same arguments used above for normal galaxies, while the difference in the UV band can be due to an increasing contribution from a population of young stars, or the active nucleus. The emission in the X-ray has some spread due to the large aperture.

The SBLs and SBHs have similar SEDs along the entire energy spectrum. The SBLs have a small spread in the UV, while for SBHs the most noticeable spread is in the radio and far-IR bands. The X-ray emission, contrary to what is ob-

TABLE 4. List of References of Tables 3 and 5.

1—Aaronson 1977
2—Allen 1976
3—Artyukh & Ogannisyam 1983
4—Balzano & Weedman 1981
5—Bartel *et al.*1982
6—Batuski *et al.* 1992
7—Baum *et al.* 1993
8—Biermann *et al.* 1980
9—Boller *et al.* 1992
10—Calzetti 1997
11—Buczilowski 1988
12—Cameron 1971
13—Condon 1980
14—Condon 1983
15—Condon 1987
16—Condon & Broderick 1988
17—Condon & Broderick 1991
18—Condon *et al.* 1991
19—Condon *et al.* 1990
20—Condon & Jaucey 1974
21—Cox *et al.* 1988
22—Deeg *et al.* 1993
23—Dennison *et al.* 1975
24—deVaucoulers & Longo 1988
25—Dressel & Condon 1978
26—Dyck *et al.* 1978
27—Ellis *et al.* 1982
28—Fabbiano *et al.* 1992
29—Ficarra *et al.* 1985
30—Forbes & Ward 1993
31—Frogel *et al.* 1982
32—Frogel *et al.* 1978
33—Gallagher *et al.* 1982
34—Genzel *et al.* 1976
35—Glass 1973
36—Glass 1976
37—Glass 1978
38—Glass 1979
39—Glass 1981
40—Glass 1984
41—Glass & Moorwood 1985
42—Gregory & Condon 1991
43—Griersmith *et al.* 1982
44—Harnett 1982
45—Harnett 1984
46—Harnett 1987
47—Heidmann *et al.* 1982
48—Hummel 1980
49—Hummel *et al.* 1984
50—Hunter & Gallagher 1985
51—Israel & Mahoney 1990
52—Israel *et al.* 1992
53—Israel & van der Hulst 1983
54—Joyce & Simon 1976
55—Kelermann *et al.* 1969
56—Klein *et al.* 1983
57—Klein & Gräve 1986
58—Klein *et al.* 1991
59—Klein *et al.* 1984
60—Kleinmann & Wright 1974
61—Knapp *et al.* 1989
62—Kojoian *et al.* 1980
63—Kollatschny *et al.* 1983
64—Kühr *et al.* 1981
65—Lawrence *et al.* 1991
66—Lebofski & Rieke 1979
67—Longmore & Sharples 1982
68—McAlary *et al.* 1979
69—Meurs & Wilson 1984
70—Moorwood & Glass 1982
71—Morris *et al.* 1985
72—Oly & Israel 1993
73—Ondrechen 1985
74—Pauliny-Toth *et al.* 1978
75—Penston 1973
76—Persson *et al.* 1980
77—Persson *et al.* 1979
78—Pilkington *et al.* 1965
79—Rieke 1978
80—Rieke & Lebofsky 1978
81—Rieke & Low 1972
82—Rudy *et al.* 1982
83—Sadler 1984
84—Sadler *et al.* 1989
85—Sanamyan *et al.* 1983
86—Sandage *et al.* 1969
87—Schommer *et al.* 1988
88—Skilman & Klein 1988
89—Slee & Higgins 1973
90—Sramek & Weedman 1986
91—Stothers & Chin 1972
92—Stull 1971
93—Subrahmanya & Harnett 1987
94—Telesco & Gatley 1981
95—Thronson *et al.* 1987
96—Tovmassian *et al.* 1984
97—Tovmassian & Terzian 1974
98—Ulvestad & Wilson 1984a
99—Ulvestad & Wilson 1984b
100—Ulvestad & Wilson 1989
101—Unger *et al.* 1986
102—van Driel *et al.* 1991
103—Vila *et al.* 1990
104—Ward *et al.* 1980
105—Ward *et al.* 1982
106—Wills 1975
107—Wright *et al.* 1974
108—Wright & Otrupcek 1990
109—Wynn-Williams 1986
110—Thuan 1983

served for the rest of the galaxies, drops abruptly relative to the UV emission in both types of starburst galaxies. The emission in the X-ray comes mostly from SNR, concentrated in the Starburst region.

5. COMPARISON BETWEEN DIFFERENT SEDs

In Fig. 4 we make a comparison between objects of similar activity class, normalized again at λ7000 Å. On the bottom panel we compare the average SED of normal ellipticals and spirals. The two groups are very similar from the radio to the visual waveband. The most significant difference is in the ultraviolet part of the spectrum, where the spirals have an increasing contribution from H II regions. The apparent large difference at log $\nu \approx 13.5$ may be due to the fact that at this waveband, flux was available only for some of the ellipticals and for no spirals. Likewise, the difference in the X-ray fluxes is uncertain due to the small number of spirals with available X-ray fluxes.

On the middle panel we compare the SEDs of LINER's and Seyfert 2's. The two SEDs overlap only in the visual to near-IR region ($14 < \log \nu < 15$), where they are dominated by the old stellar population, differing in all other wavebands (but see below, where LINER's and Seyfert 2's are compared using different normalizations). The UV and X-ray emission of Seyfert 2's is larger than that of LINER's, consistent with a larger contribution from the active nucleus, or in some cases, the presence of a circumnuclear H II region. The Seyfert 2's are also brighter than LINER's in the mid/far-IR and radio wavebands. Most of the IR emission in Seyfert 2's is probably due to reradiation of the nuclear emission by a circumnuclear torus (Storchi-Bergmann *et al.* 1992), which is possibly not present in LINER's. The higher radio emission from the Seyfert 2's can be explained by the higher nuclear activity of these objects.

On the top panel of Fig. 4 we compare the SEDs of SBHs and SBLs. These two SEDs are very similar along the entire energy spectrum. The only differences are in the ultraviolet, where the SBL's are brighter than SBH's due to the lower reddening, and in the mid/far-IR, where SBH's are brighter than SBL's. This behaviour was studied by Calzetti *et al.* (1995), who found that the energy absorbed in the UV is reradiated in the mid/far-IR.

In Fig. 5 we show the comparison among groups of different activity class. On the top left panel we plot the Seyfert 2's, SBL's, and SBH's SEDs. These SEDs are similar from the radio to near-IR waveband. However, they start to diverge in the visual towards UV wavelengths. In this waveband the Seyfert 2's are dominated by the old stellar population and have the reddest energy distribution, probably due to the obscuration of the AGN continuum by the torus, while SBHs and SBLs are increasingly bluer, and dominated by the young stellar population. These SEDs also differ in the X-ray waveband where the Seyfert 2's are brighter. On the top right panel we show the LINER's, SBH's, and SBL's SEDs. The only wavelength region where these SEDs are similar is from the visual to the near-IR, where they are normalized. The LINER's SED is systematically fainter at all other bands.

On the bottom left panel of Fig. 5 we show the SEDs of LINER's, Seyfert 2's, and Spirals. The LINER's and Spirals have similar SEDs, only differing in the mid/far-IR and UV, where the Spirals are fainter than the LINER's. Seyfert 2's and Spirals SEDs are similar only in the near-IR to visual waveband, where they are dominated by the old stellar population. The Seyfert 2's are much brighter than the Spirals in the IR and UV. The SEDs of Spirals, SBL's and SBH's are compared on the bottom right panel of Fig. 5. Here we can see the difference between SEDs dominated by old (Spirals)

TABLE 5. Millimeter, IR, and X-ray data.

Name Freq. (10^{12} Hz) Apert.	mm	20 μm 15	10 μm 30	5 μm 60	3.5 μm 86	2.2 μ 136	1.6 μm 188	1.2 μm 250	X-ray E band (KeV)	Refs.
NGC221			89		412	795	1010	1210		81, 75, 75,
			28.6		85.7	136	182	240		75, 32
			6″		9.6″	10.6″	10.6″	16″		
NGC224			25	59	750	1030	1280	1020		80, 80, 86,
			30	62.5	88.2	136	182	240		76, 76, 76
			5.7″	5.9″	15″	13.7″	13.7″	13.7″		
IC1586						6.57	8.32	7.4		4, 4, 4
						135	181	244		
						8.5″	8.5″	8.5″		
NGC262	360		300		39	22	17	14		54, 79, 79,
	0.091		28.3		86.9	135	184	240		79, 79, 79
	75″		5.7″		8.5″	8.5″	8.5″	8.5″		
HARO15						9.82	13.85	13.00		50, 50, 50
						135	182	240		
						23″	23″	23″		
MRK357						3.28	3.26	2.82		10, 10, 10
						135	182	240		
						10″	10″	10″		
NGC598						23.6	33.1		161.2	33, 33, 28
						135	181		0.2–4.0	
						9.8″	9.8″			
IC214						16.6	17.12	13.35		10, 10, 10
						135	182	240		
						10″	10″	10″		
NGC1023						244	312	254		10, 10, 10
						136	182	240		
						48″	48″	48″		
NGC1068	170	66000	25000	3200	1720	668	531	372	195.3	95, 66, 91, 81,
	0.23	14.3	30	60	85.7	137	183	250	0.2–4.0	39, 39, 39, 39,
	33″	8.5″	6″	6″	12″	12″	12″	12″		28
NGC1097		240	65		301	308	360	277	30.3	94, 94, 35,
		15	29.4		85.7	137	183	250	0.2—4.0	43, 43, 43,
		5″	5″		25.2″	22″	22″	22″		28
NGC1140						28.8	39.9	37.5		50, 50, 50
						135	182	240		
						23″	23″	23″		
NGC1313									18.9	28
									0.2–4.0	
NGC1316					150	314	360	349	11.6	35, 35, 35, 35,
					85.7	137	183	250	0.2–4.0	28
					12″	12″	12″	12″		
NGC1399						153	190	149	229.43	67, 67, 67,
						136	182	240	0.2–4.0	28
						12″	12″	12″		
NGC1404						156	199	168	33.22	67, 67, 67
						136	182	240	0.2–4.0	28
						12″	12″	12″		
NGC1433						150	187	167		35, 35, 35
						137	183	250		
						18″	18″	18″		
NGC1553					222	279	381	336	14.35	36, 36, 36,
					88.2	137	183	250	0.2–4.0	36, 28
					18″	18″	18″	18″		
NGC1672					203	186	211	151	7.65	35, 35, 35, 35,
					85.7	137	183	250	0.2–4.0	28
					12″	12″	12″	12″		
NGC1667						33.73	39.94	31.44		10, 10, 10
						135	182	240		
						10″	10″	10″		
NGC3031		310	150			1250	1600	1220	58.94	26, 26,
		15	30			135	182	242	0.2–4.0	1, 1, 1, 28
		6.8″	6.8″			20.6″	20.6″	20.6″		
NGC3049						7.2	9.56	6.56		4, 4, 4
						135	181	244		
						10.3″	10.3″	10.3″		

TABLE 5. (continued)

Name Freq. (10^{12} Hz) Apert.	mm	20 μm 15	10 μm 30	5 μm 60	3.5 μm 86	2.2 μ 136	1.6 μm 188	1.2 μm 250	X-ray E band	Refs.
NGC3081					37.1	28.1	31.7	24.6	8.09	105, 105, 105,
					78.9	137	183	250	0.2–4.0	105, 28
					7″	7″	7″	7″		
NGC3256					142	200	123	129	34.5	35, 35, 35,
					85.7	137	183	250	0.1–2.4	35, 9
					25.2″	25.2″	25.2″	25.2″		
NGC3660									10.6	28
									0.2–4.0	
NGC4385			240		15.1	24.2	32.8	16.9	<7.43	81, 2, 2,
			28.6		84.7	135	181	244	0.2–4.0	2, 4, 28
			6″		17″	17″	17″	10.3″		
NGC4569			170		218	111	137	115	6.0	81, 24, 4,
			28.6		84.7	135	181	244	0.2–4.0	4, 4, 28
			6″		10″	10.3″	10.3″	10.3″		
NGC4579						247	316	243	48.13	1, 1, 1,
						135	182	242	0.2–4.0	28
						20.6″	20.6″	20.6″		
NGC4594					319	565	737	516	29.24	27, 27, 27,
					84.7	135	187	238	0.2–4.0	27, 28
					14.4″	14.4″	14.4″	14.4″		
IC3639						23.4	25.9	20.5		105, 105, 105
						137	183	250		
						7″	7″	7″		
NGC5135					55.2	69.8	75.4	51.7	3.35	41, 41, 41,
					85.7	135	182	250	0.2–4.0	41, 28
					12″	12″	12″	12″		
NGC5236[a]		3590	1110		197	305	414	307	47.0	31, 31, 35,
		15	28.8		85.7	137	183	250	0.2–4.0	35, 35, 35, 28
		12.6″	12.6″		12″	12″	12″	12″		
NGC5253[b]		6100	1540		86.1	33.5	28.9	30.6	2.17	31, 31, 35,
		15	28.8		85.7	137	183	240	0.2–4.0	35, 35, 70, 28
		8.2″	8.2″		12″	12″	12″	12″		
NGC5506	31				349	152	75.3	36.6	111.83	65, 37, 38,
	0.2773				88.2	137	183	250	0.2–4.0	37, 38, 28
	19″				12″	12″	12″	12″		
NGC5643					34.5	66.1	80.4	60.5	10.5	41, 41, 41,
					85.7	135	182	240	0.2–4.0	41, 28
					12″	12″	12″	12″		
MRK477						12.0	12.9	5.2		2, 2, 82
						136	182	240		
						17″	17″	8.5″		
NGC5728					44	75	89	70	5.46	68, 68, 68,
					82.1	135	181	244	0.2–4.0	68, 28
					15″	15″	15″	15″		
UGC9560						1.87	2.52	2.39		110, 110, 110
						135	182	240		
						7.8″	7.8″	7.8″		
NGC5860						11.07	13.98	11.63		10, 10, 10
						135	182	240		
						10″	10″	10″		
NGC5996						8.5	10.7	8.81		4, 4, 4
						135	181	244		
						8.5″	8.5″	8.5″		
NGC6052					10.5	8.12	10.6	9.23	<10.4	2, 4, 4, 4,
					84.7	135	181	244	0.2–4.0	28
					17″	10.3″	10.3″	10.3″		
NGC6090						16.00	16.80	13.85		10, 10, 10
						135	182	240		
						10″	10″	10″		
NGC6217						34.5	38.7	32.6		4, 4, 4
						135	181	244		
						10.1″	10.1″	10.1″		
NGC6764			150		11	16	15	12.5		79, 79, 79,
			28.3		86.9	135	184	240		79, 79
			5.7″		8.5″	8.5″	8.5″	8.5″		

TABLE 5. (continued)

Name	mm	20 μm	10 μm	5 μm	3.5 μm	2.2 μ	1.6 μm	1.2 μm	X-ray	Refs.
Freq. (10^{12} Hz)		15	30	60	86	136	188	250	E band	
Apert.										
NGC6868						273	349	292		77, 77, 77
						135	182	240		
						33.6″	33.6″	33.6″		
NGC7130						102.8	115.2	85.8		41, 41, 41
						135	182	240		
						34″	34″	34″		
NGC7196						148.6	185.9	141.1		40, 40, 40
						135	182	240		
						18″	18″	18″		
NGC7250						9.64	12.06	11.00		10, 10, 10
						135	182	240		
						10″	10″	10″		
NGC7496					21.6	38.4	42.6	31.7	<4.45	41, 41, 41,
					86.9	135	182	240	0.2–4.0	41, 28
					9″	18″	18″	18″		
NGC7552[c]		4630	1020		214	174	198	144	8.74	31, 31, 36,
		15	28.8		88.2	137	183	250	0.2–4.0	36, 36, 36, 28
		12.6″	12.6″		12″	12″	12″	12″		
NGC7582[d]		2850	510		192	174	156	102	11.09	31, 31, 36,
		15	28.8		88.2	137	183	250	0.2–4.0	36, 36, 36, 28
		8.2″	8.2″		12″	12″	12″	12″		
NGC7590						143.2	180.9	139.8	2.83	41, 41, 41, 28
						135	182	240	0.2–4.0	
						34″	34″	34″		
NGC7673						10.86	13.47	12.40	2.78	10, 10, 10, 28
						135	182	240	0.2–4.0	
						10″	10″	10″		
NGC7714			250			27.4	33.4	27.1	2.82	81, 4, 4, 4,
			28.6			135	181	244	0.2–4.0	28
			6″			8.5″	8.5″	8.5″		
MRK542						5.65	6.63	5.83		10, 10, 10
						135	182	240		
						10″	10″	10″		
NGC7793			430			18	21.5	31.1	6.81	60, 91, 91,
			28.3			137	183	250	0.2–4.0	91, 28
			17″			12″	12″	12″		

The fluxes listed in this Table are given in mJy, except those of the x-ray band, which are given in 10^{-13} ergs cm^{-2} s^{-1}. The references number is related to Table 4. The following galaxies also have some more IR data:

[a]NGC 5236: 2.63×10^{13} Hz=1090 mJy (12.6″) (Ref. 31); 3.12×10^{13} Hz=657 mJy (12.6″) (Ref. 31); 3.49×10^{13} Hz=1150 mJy (12.6″) (Ref. 31); 3.84×10^{13} Hz=1980 mJy (12.6″) (Ref. 31).
[b]NGC 5253: 1.72×10^{13} Hz=5500 mJy (7.5″) (Ref. 70); 2.42×10^{13} Hz=2040 mJy (8.2″) (Ref. 31); 2.63×10^{13} Hz=1570 mJy (8.2″) (Ref. 31); 3.12×10^{13} Hz=1070 mJy (8.2″) (Ref. 31); 3.49×10^{13} Hz=817 mJy (8.2″) (Ref. 31); 3.84×10^{13} Hz=866 mJy (8.2″) (Ref. 31).
[c]NGC 7552: 2.42×10^{13} Hz=1780 mJy (12.6″) (Ref. 31); 2.63×10^{13} Hz=1340 mJy (12.6″) (Ref. 31); 3.12×10^{13} Hz=465 mJy (12.6″) (Ref. 31); 3.49×10^{13} Hz=1270 mJy (12.6″) (Ref. 31); 3.84×10^{13} Hz=1850 mJy (12.6″) (Ref. 31).
[d]NGC 7582: 2.42×10^{13} Hz=1070 mJy (8.2″) (Ref. 31); 2.63×10^{13} Hz=671 mJy (8.2″) (Ref. 31); 3.12×10^{13} Hz=337 mJy (8.2″) (Ref. 31); 3.49×10^{13} Hz=711 mJy (8.2″) (Ref. 31); 3.84×10^{13} Hz=1140 mJy (8.2″) (Ref. 31).

and young stellar populations (SBH's and SBL's). The only wavelength region where these SEDs can be considered similar is in the visual to near-IR, again the region where they are normalized. In these region the starbursts have some contribution from old stars. The Spirals are fainter in any other waveband.

In Fig. 6 we compare the SEDs of LINER's and Seyfert 2's (top), SBL's and SBH's (bottom) with those of radio quiet and radio loud quasars from Sanders *et al.* (1989) (RQQ and RLQ hereafter). In contrast to the previous analysis, here the SEDs were normalized to the 60 μm flux. We chose λ60 μm as normalization wavelength because this is the wavelength region that is the most isotropic in the entire quasars SED (Pier & Krolik 1992). We could not find an average SED for Seyfert 1's, but a comparison between the RQQ SED with that of the Seyfert 1 galaxy NGC 3783 (Alloin *et al.* 1995), showed that they are very similar.

The comparison between the SEDs of quasars and the other galaxies shows that quasars are $\approx$0.5 dex brighter in the mid/far-IR, $\approx$1 dex brighter in the near-IR, and $\approx$2 to 2.5 dex brighter in the visual to X-ray region of the spectrum. The only exception to the above differences are for LINER's in the visual to near-IR region of the spectrum, whose SEDs touch those of the quasars. This is due to the fact that the nuclear luminosity of LINER's, i.e., the energy emitted from the nuclear engine is much smaller than that of quasars. When the SEDs are normalized to the radiation that is emitted isotropically from the nucleus (60 μm), the

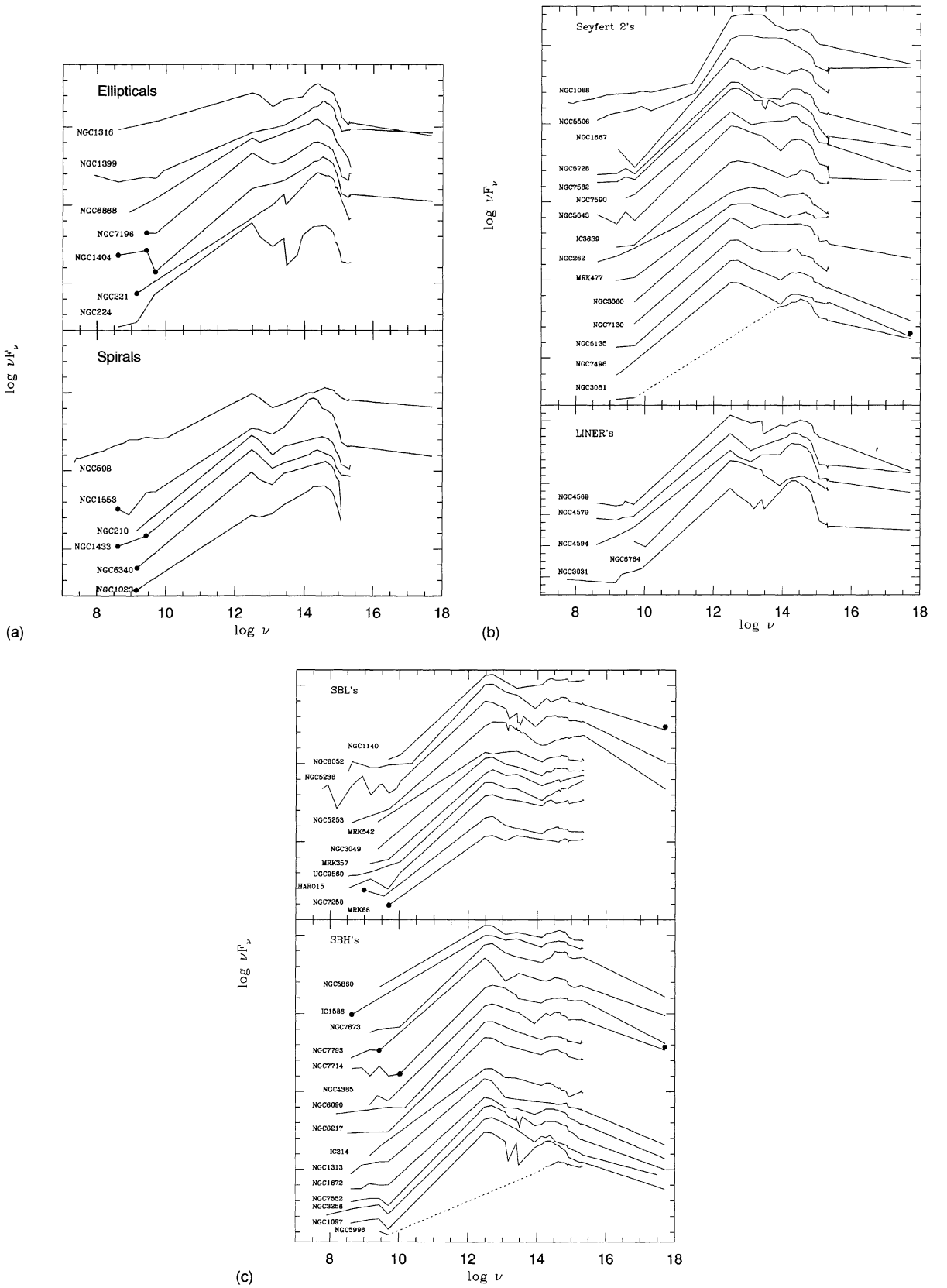

FIG. 1. Individual SEDs, separated by arbitrary constants. The galaxy name is shown on the left of each SED. The dashed lines represent regions for which there were no Iras data available. (a) Normal ellipticals (top) and spirals (bottom); (b) Seyfert 2's (top) and LINER's (bottom); (c) low reddening Starburst's (top) and high reddening Starbursts (bottom).

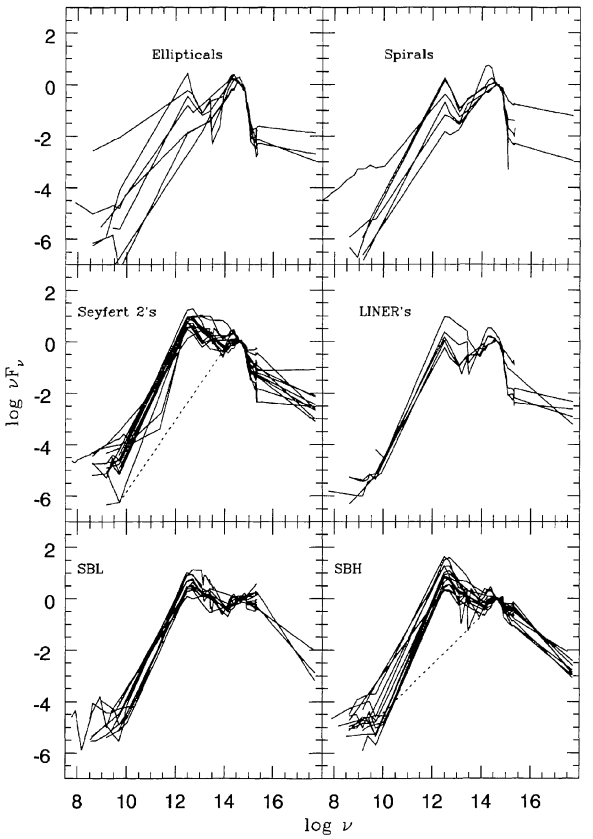

FIG. 2. Plot of individual SEDs, normalized to the flux at 7000 Å, of normal ellipticals (top left), normal spirals (top right), Seyfert 2's (middle left), LINER's (middle right), low reddening Starbursts (bottom left) and high reddening Starbursts (bottom right).

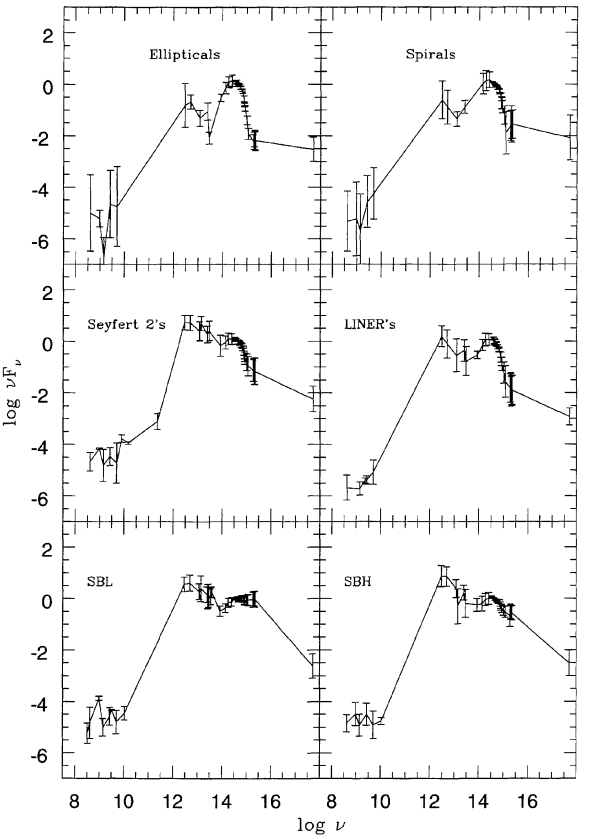

FIG. 3. Plot of the average SEDs, using the same order as Fig. 2. The error bars are the standard deviation of the average.

near-IR and visual regions of the SEDs of LINER's, which are dominated by the stellar population in these objects, will be shifted to values comparable to those of quasars. In the radio waveband, the RQQ's SED is similar to that of Seyfert 2's, starbursts and LINER's, while the RLQ's SEDs are $\approx$3 dex brighter than all others. From Fig. 6 we see that the RQQ and RLQ SEDs are dominated by the visual and UV emission, which is due to the nuclear featureless continuum. As opposed to the Seyfert 2's, LINER's and starbursts, quasars do not have a pronounced mid/far-IR emission bump relative to the visual and UV parts of the spectrum.

Another interesting fact to be noticed in this figure is the similarity between the SEDs of Seyfert 2's and LINER's, when we normalize them to the 60 μm flux. With the exception of the visual and near-IR region of the spectrum where, due to their low nuclear luminosity LINER's are dominated by the stellar population, the two SEDs are very similar, suggesting that LINER's are indeed low luminosity relatives of Seyferts.

6. THE SED OF H II REGIONS AND SUPERNOVA REMNANTS

Here we describe the SED of H II regions, a thermal and a non-thermal supernova remnant (SNR). These SEDs can be compared with those from starbursts, in order to determine the wavebands where the young components contribute most to the SED.

As examples of single H II regions we use NGC 5455, NGC 5461, and NGC 5471, in the disk of M101, and NGC 604 in the disk of M33. These objects are bright, have sizes of 30″ typically, and are not resolved into stars, which make them ideal for our analysis. Their metallicities are subsolar, $12+\log O/H=8.51$, 8.28, 8.31, and 8.05 for NGC 604, NGC 5455, NGC 5461, and NGC 5471, respectively (Garnett 1989; Torres-Peimbert *et al.* 1989). For the non-thermal SNR we use the Crab nebula, which is a close and well studied object, while for the thermal SNR we use N49 in the LMC, which is relatively compact and bright.

The X-ray fluxes of the H II regions, observed with *ROSAT*, were obtained from Williams & Chu (1995) for the objects in M101 and Schulman & Bregman (1995) for the objects in M33. The UV fluxes, observed with IUE, were measured from Figs. 6, 29, 30, and 32 of Rosa *et al.* (1984) for NGC 604, NGC 5455, NGC 5461, and NGC 5471, respectively. The radio fluxes at 1.47 GHz and 4.89 GHz were obtained from Sramek & Weedman (1986), and are integrated over the entire H II region. The mid/far-IR (*IRAS*) fluxes were obtained from NED. The near-IR fluxes (J, H, and K) of NGC 5455 and NGC 5471 were obtained from Campbell & Terlevich (1984), observed with an aperture of 10″. For NGC 5461 we use the values from Blitz *et al.* (1981), obtained with an aperture of 10″, while for NGC 604

TABLE 6. Average SEDs.

Log ν	Ellip.	σ	Spir.	σ	LINER	σ	Sy2	σ	SBL	σ	SBH	σ
8.61	−4.99	1.48	−5.31	1.16	−5.67	0.49	−4.67	0.36	−4.84	0.61	−4.84	0.33
8.98	−5.21	0.32	−5.22	1.43	...	...	−4.16	0.03	−3.88	0.08	−4.48	0.45
9.15	−6.72	0.79	−5.67	1.41	−5.72	0.26	−4.81	0.63	−5.00	0.34	−4.92	0.43
9.36	...	...	...	...	−5.41	0.10	...	...	...	...	...	...
9.43	−4.65	1.31	−4.56	1.00	−5.38	0.16	−4.47	0.35	−4.58	0.34	−4.50	0.43
9.7	−4.75	1.56	−4.23	1.00	−5.07	0.47	−4.72	0.77	−4.81	0.46	−4.90	0.53
9.90	...	...	...	...	...	...	−3.78	0.15	...	...	...	...
10.17	...	...	...	...	...	...	−3.95	0.05	−4.45	0.26	−4.76	0.13
11.36	...	...	...	...	...	...	−3.10	0.31	...	...	...	...
12.48	−0.81	0.85	−0.61	0.73	0.19	0.41	0.74	0.28	0.56	0.28	0.88	0.41
12.70	−0.68	0.27	−0.88	0.66	−0.10	0.55	0.73	0.29	0.61	0.31	0.87	0.38
13.08	−1.31	0.31	−1.35	0.28	−0.54	0.63	0.41	0.37	0.28	0.31	0.40	0.35
13.15	...	...	...	...	...	...	0.70	0.28	0.40	0.50	−0.30	0.68
13.40	−1.05	0.33	−0.88	0.25	−0.36	0.41	0.28	0.32	0.17	0.30	0.22	0.28
13.46	−2.09	0.23	...	...	−0.76	0.56	0.42	0.38	0.13	0.46	−0.19	0.54
13.93	−0.52	0.14	...	...	−0.53	0.14	−0.16	0.41	−0.48	0.20	−0.25	0.25
14.14	−0.14	0.22	0.02	0.40	−0.15	0.22	−0.03	0.25	−0.36	0.16	−0.20	0.29
14.26	0.08	0.21	0.14	0.39	0.06	0.24	0.10	0.23	−0.16	0.18	−0.04	0.23
14.40	0.15	0.22	0.17	0.31	0.07	0.23	0.10	0.21	−0.12	0.17	0.01	0.24
14.53	0.12	0.02	0.10	0.01	...	...	0.12	0.05	−0.00	0.05	0.06	0.04
14.56	0.08	0.02	0.06	0.01	...	...	0.07	0.05	−0.01	0.03	0.03	0.02
14.60	0.09	0.09	0.04	0.01	0.04	0.12	0.06	0.07	0.01	0.06	0.02	0.02
14.66	0.00	0.06	−0.04	0.02	−0.04	0.11	−0.02	0.08	−0.03	0.09	−0.02	0.03
14.69	−0.02	0.06	−0.05	0.03	−0.09	0.09	−0.04	0.08	0.01	0.07	−0.04	0.03
14.71	−0.04	0.05	−0.08	0.03	−0.12	0.08	−0.06	0.09	0.02	0.07	−0.06	0.04
14.75	−0.13	0.07	−0.16	0.04	−0.21	0.08	−0.13	0.10	0.01	0.07	−0.09	0.06
14.81	−0.23	0.06	−0.24	0.07	−0.31	0.09	−0.16	0.12	0.04	0.09	−0.10	0.08
14.82	−0.27	0.07	−0.28	0.09	−0.34	0.08	−0.23	0.13	0.03	0.09	−0.12	0.08
14.87	−0.55	0.11	−0.48	0.15	−0.52	0.11	−0.36	0.18	0.03	0.10	−0.17	0.12
14.89	−0.79	0.06	−0.72	0.24	−0.61	0.19	−0.45	0.21	−0.02	0.11	−0.26	0.13
14.91	−0.79	0.09	−0.73	0.21	−0.78	0.16	−0.58	0.21	−0.09	0.12	−0.35	0.13
14.93	−0.93	0.11	−0.88	0.24	−0.89	0.25	−0.67	0.22	−0.09	0.16	−0.39	0.15
15.01	−1.39	0.17	−1.20	0.36	−1.21	0.41	−0.80	0.32	−0.05	0.19	−0.46	0.19
15.07	−1.91	0.22	−1.89	0.82	−1.57	0.61	−0.95	0.38	−0.05	0.22	−0.50	0.21
15.28	−2.23	0.28	−1.62	0.58	−1.83	0.55	−1.13	0.41	−0.04	0.29	−0.68	0.41
15.30	−2.13	0.28	−1.48	0.64	−1.84	0.61	−1.10	0.45	0.02	0.28	−0.51	0.29
15.31	−2.14	0.38	−1.64	0.60	−1.95	0.58	−1.14	0.51	0.01	0.28	−0.54	0.28
15.35	−2.19	0.37	−1.55	0.55	−1.90	0.57	−1.16	0.51	−0.02	0.30	−0.56	0.28
17.71	−2.52	0.47	−2.08	0.87	−2.86	0.33	−2.24	0.50	−2.62	0.48	−2.51	0.50

we use the values from Hunter & Gallagher (1985), observed with an aperture of 23″.

The visual fluxes of NGC 604 were measured from Fig. 6 of D'Odorico *et al.* (1983). They observed several parts of the H II region, with apertures of 4″×8″, and give the sum of these observations, which corresponds to an aperture similar to that of *IUE*. For NGC 5455, NGC 5461, and NGC 5471, the visual fluxes were calculated from Torres-Peimbert *et al.* (1989), using their emission-line fluxes and equivalent widths. Their aperture was 3.8″×12.4″, which corresponds to ≈25% of the *IUE* aperture, but include the H II region peak emission.

The SED of the Crab nebula was obtained from Woltjer (1987) and is described by the following relations. For $7<\log\nu<12$, $\log\nu F_\nu = 5.717+0.7\times\log\nu$; for $13.3<\log\nu<15.5$, $\log\nu F_\nu = 13.01+0.15\times\log\nu$; and for $16<\log\nu<19$, $\log\nu F_\nu = 17.797-0.15\times\log\nu$. The flux densities ($\nu F_\nu$) in the *IRAS* bands were measured from Fig. 4 in that paper and are: 15.08, 15.15, 15.06, and 14.88 for the wavebands 12, 25, 60, and 100 μm, respectively.

The radio data of N49 were obtained from Wright & Otrupcek (1990) and are 2.73 Jy (0.48 GHz), 1.16 Jy (2.7 GHz), 0.63 Jy (5.0 GHz), and 0.47 Jy (8.4 GHz). The mid/far-IR (*IRAS*) fluxes are 0.56 Jy (12 μm), 1.78 Jy (25 μm), 19.5 Jy (60 μm), and 41.6 Jy (100 μm) (Schwering & Israel 1990).

X-ray, UV, and visual fluxes of N49 were obtained from Vancura *et al.* (1992). The X-ray flux, observed with *Einstein* and integrated over the entire SNR, is 6.34×10^{-11} erg cm^{-2} s^{-1}. The flux in the visual band, obtained from a narrow-band image centered at λ6100 Å and corrected for internal reddening ($E(B-V)=0.35$) using the extinction law of Fitzpatrick (1986), is 3.85×10^{-14} erg cm^{-2} s^{-1} Å^{-1}. In order to obtain the UV fluxes for the entire SNR we use the fact that the λ6100 Å flux inside Vancura *et al.* (1992) "A" *IUE* aperture is 10% that of the entire nebula, and assume that this percentage is equal for the UV waveband. The UV fluxes of the "A" aperture were measured from their Fig. 6, multiplied by 10, and corrected for internal reddening. The final fluxes are 4.63×10^{-12}, 1.1×10^{-12} and 4.87×10^{-13} erg cm^{-2} s^{-1} Å^{-1} for 1350, 2200, and 2900 Å, respectively.

The fluxes of individual H II regions, as well as the average SED of H II regions, N49 and Crab nebula are given in

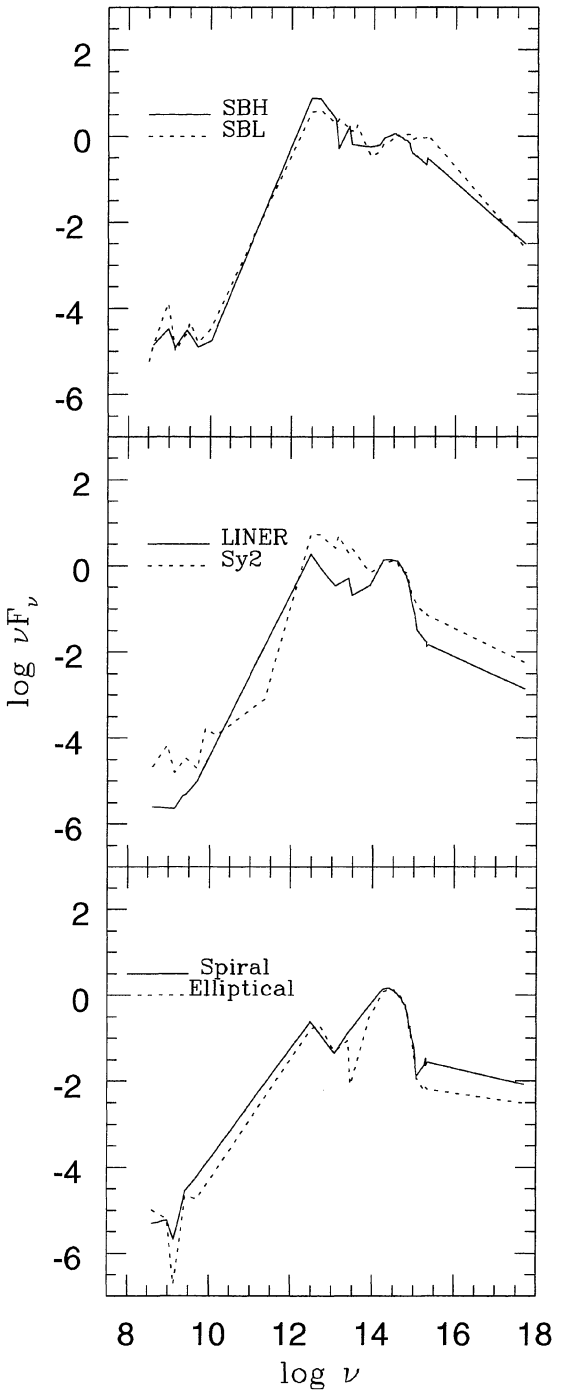

FIG. 4. Comparison between the average SED of normal ellipticals and Spirals (bottom); Seyfert 2's and LINER's (middle); and high and low reddening Starbursts (top).

Table 7. We show in Fig. 7 the individual H II regions SEDs normalized to the flux at λ7000 Å. These SEDs are very similar along the entire energy spectrum, showing a steep ultraviolet continuum, a small bump in the near-IR (log $\nu \approx 14$ Hz) and a large bump in the mid/far-IR. However, the near-IR bump is uncertain, due to the different apertures through which the visual and near-IR data were obtained. This same problem may be affecting the mid/far-IR

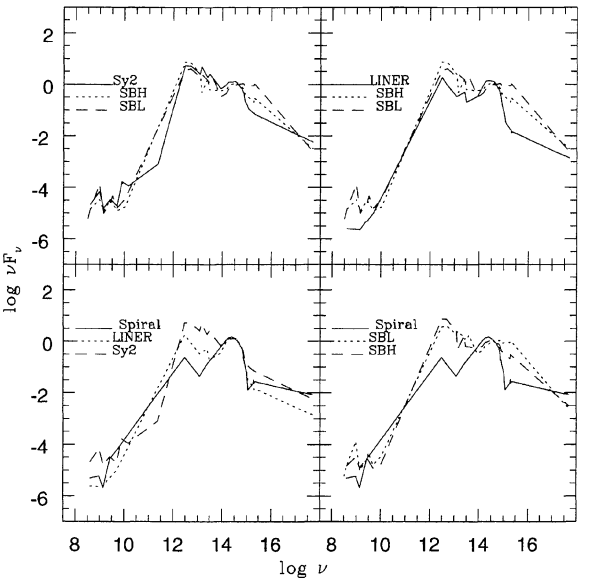

FIG. 5. Comparison between the average SED of Seyfert 2, high and low reddening Starbursts (top left); LINER's, high and low reddening Starbursts (top right); normal spirals, LINER's and Seyfert 2's (bottom left); and normal spirals, high and low reddening Starbursts (bottom right).

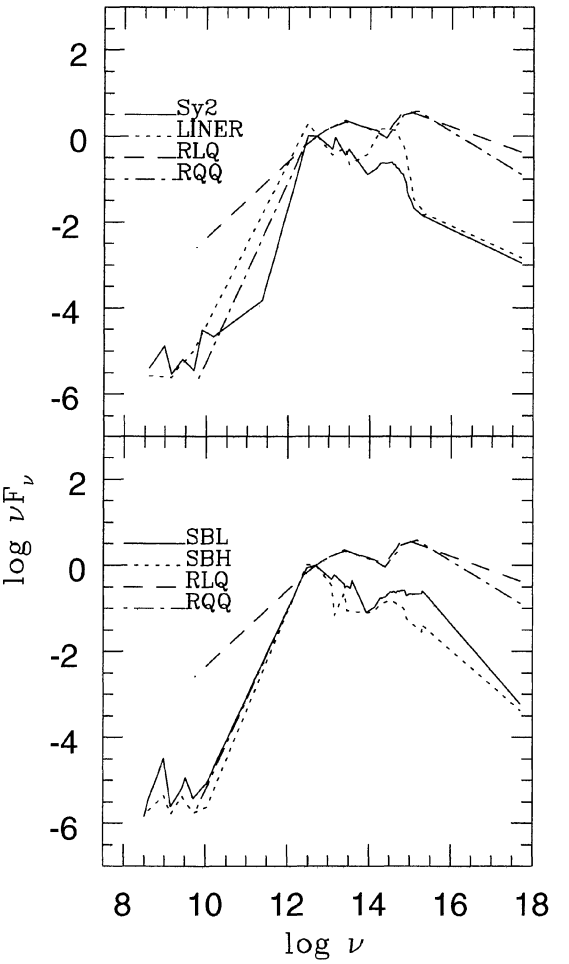

FIG. 6. Comparison of the SED of Seyfert 2's and LINER's with radio quiet and radio loud quasars from Sanders *et al.* (1989), normalized to the flux at λ60 μm (top); high and low reddening Starbursts with radio quiet and radio loud quasars (bottom).

TABLE 7. H II regions fluxes, SNRs and average H II SEDs.

	Fluxes				SEDs			
Log ν	NGC 5455	NGC 5461	NGC5471	NGC604	H II regions	σ	N49	Crab
17.71	...	...	...	...	...	...	−1.05	−0.06
17.51	7.64×10^{-14}	4.70×10^{-14}	2.78×10^{-14}	11.9×10^{-14}	−2.50	0.14	...	...
15.35	4.00×10^{-14}	3.00×10^{-14}	9.20×10^{-14}	23.0×10^{-14}	0.97	0.15	1.43	0.11
15.32	3.80×10^{-14}	2.60×10^{-14}	8.00×10^{-14}	20.0×10^{-14}	0.95	0.16	...	...
15.28	3.60×10^{-14}	3.00×10^{-14}	7.00×10^{-14}	18.0×10^{-14}	0.97	0.13	...	...
15.13	...	...	...	...	...	...	1.00	...
15.07	1.20×10^{-14}	1.00×10^{-14}	2.20×10^{-14}	7.00×10^{-14}	0.71	0.11	...	...
15.01	1.00×10^{-14}	1.00×10^{-14}	1.80×10^{-14}	5.00×10^{-14}	0.69	0.12	0.79	...
14.91	0.32×10^{-14}	0.44×10^{-14}	0.41×10^{-14}	...	0.36	0.08		0.05
14.83	0.16×10^{-14}	0.28×10^{-14}	0.28×10^{-14}	1.45×10^{-14}	0.20	0.05	...	...
14.79	0.12×10^{-14}	0.18×10^{-14}	0.20×10^{-14}	1.35×10^{-14}	0.10	0.05	...	...
14.71	9.60×10^{-16}	0.12×10^{-14}	0.16×10^{-14}	0.75×10^{-14}	0.05	0.04	...	...
14.66	6.80×10^{-16}	8.50×10^{-16}	0.13×10^{-14}	...	0.02	0.03	...	...
14.62	6.30×10^{-16}	9.10×10^{-16}	0.12×10^{-14}	...	0.0	0.0	...	...
14.38	5.29×10^{-16}	7.13×10^{-16}	5.80×10^{-16}	0.35×10^{-14}	0.06	0.10	...	−0.03
14.26	2.73×10^{-16}	3.43×10^{-16}	3.06×10^{-16}	0.17×10^{-14}	−0.13	0.10	...	...
14.13	1.28×10^{-16}	2.13×10^{-16}	1.51×10^{-16}	8.46×10^{-16}	−0.28	0.11	...	...
13.40	...	8.30×10^{-16}	1.74×10^{-16}	1.87×10^{-15}	0.76	0.33	−0.22	−0.12
13.08	...	9.38×10^{-16}	1.15×10^{-16}	2.30×10^{-15}	1.07	0.42	−0.04	−0.05
12.70	...	7.98×10^{-16}	1.49×10^{-16}	2.58×10^{-15}	1.48	0.35	0.63	−0.14
12.48	...	5.50×10^{-16}	0.78×10^{-16}	2.63×10^{-15}	1.56	0.43	0.73	−0.32
9.92	...	...	...	...	...	...	−3.78	−2.54
9.69	2.00×10^{-25}	8.74×10^{-25}	6.33×10^{-25}	1.49×10^{-24}	−4.42	0.23	−3.87	...
9.43	...	...	...	...	...	...	−3.88	...
9.17	2.13×10^{-26}	7.56×10^{-26}	7.92×10^{-26}	1.28×10^{-25}	−4.89	0.24	...	...
8.68	...	...	...	...	...	...	−4.25	−3.41

The H II regions fluxes are given in units of erg cm^{-2} s^{-1} $Å^{-1}$ and the SEDs, normalized to the flux at λ7000 Å, are given in units of erg cm^{-2} s^{-1}.

bump, since the *IRAS* apertures are much larger than the H II regions and can include emission from warm and cold dust in the galaxy disk (notice that NGC 5455 do not have *IRAS* data available).

In Fig. 8 we compare the SEDs of the thermal SNR, non-thermal SNR, and average H II regions, normalized to the H II regions flux at radio 6 cm. The non-thermal SNR has a flat SED from the X-rays to the infrared waveband. It has some thermal emission in the mid-IR (Woltjer 1987) and drops towards the radio waveband. The thermal SNR has a steep UV to optical SED, like the H II regions. This emission comes from H and He recombination radiation and two photons continuum emission (Vancura *et al.* 1992). The flux drops from UV to X-ray, where it is similar to that of non-thermal SNR and stronger than H II regions. The thermal SNR SED also shows an increase in the far-IR emission due

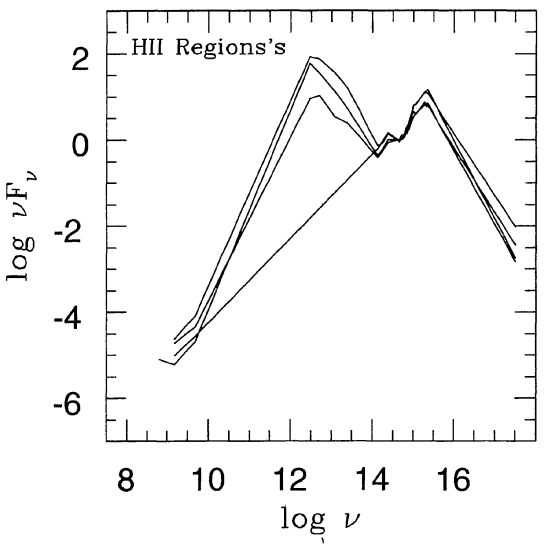

FIG. 7. SEDs of single H II regions, normalized to the flux at λ7000 Å.

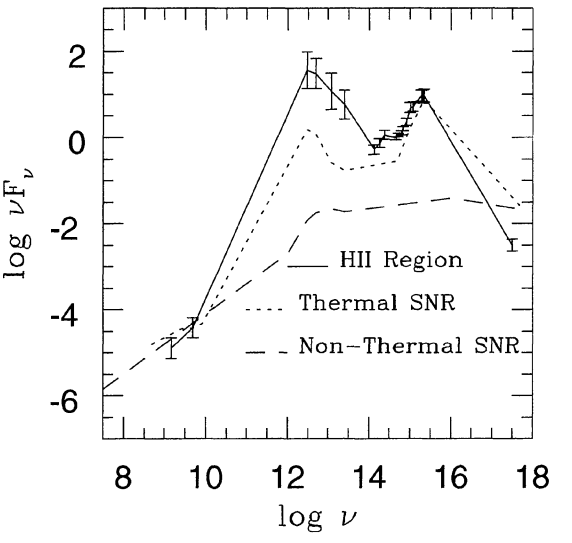

FIG. 8. SEDs of H II regions, a non-thermal SNR (Crab nebula) and a thermal SNR (N49 in the LMC), normalized to the flux at λ6 cm.

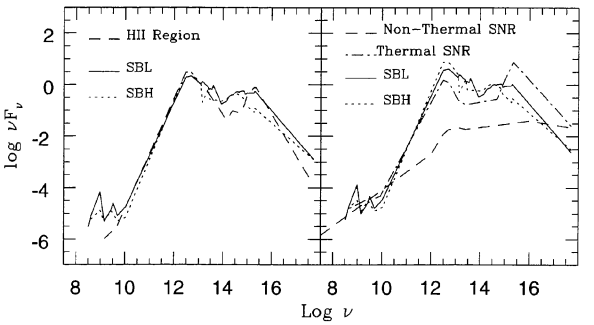

FIG. 9. The comparison of SBL and SBH SEDs with the SEDs of H II regions (left), normalized to the flux at λ25 μm, thermal and non-thermal SNR's (right), normalized to the H II region's flux at λ6 cm.

TABLE 8. Number of objects with the following ratios available.

Ratios	Ell.	Sp.	Sy2	LIN	SBL	SBH
Log (6 cm/7000 Å)	6	2	15	5	11	14
Log (100 μm/7000 Å)	6	6	14	5	11	14
Log (25 μm/7000 Å)	4	6	14	5	11	14
Log (2.2 μm/7000 Å)	7	4	14	5	10	14
Log (1.6 μm/7000 Å)	7	4	14	5	10	14
Log (1.2 μm/7000 Å)	7	4	14	5	10	14
Log (5310 Å/7000 Å)	7	6	15	5	11	15
Log (2900 Å/7000 Å)	6	6	13	5	6	10
Log (2530 Å/7000 Å)	6	6	13	5	6	10
Log (1507 Å/7000 Å)	6	3	15	4	11	15
Log (1355 Å/7000 Å)	7	4	15	4	11	15
Log (X-rays/7000 Å)	3	2	10	4	3	9

to cold dust reradiation, and then drops to the radio waveband.

In Fig. 9 we compare the SEDs of SBL's and SBH's with those of H II regions (left panel) and SNRs (right panel). The H II regions and Starbursts are normalized relative to the 25 μm flux, instead of the λ7000 Å, because the 25 μm corresponds to the warm dust emission, which should be similar in these two classes of objects. The SNRs were again normalized to the flux of H II regions at radio 6 cm (log ν=9.7).

H II regions and Starbursts have similar SEDs in the mid/far-IR parts of the spectrum, but differ in the X-ray and radio, where H II regions have smaller fluxes. In the UV part of the spectrum H II regions are similar to SBL's, but are much brighter than SBH's. However, starbursts are stronger than H II regions in the visual and near-IR parts of the spectrum. This difference is due to the fact that in H II regions we observe only the young stellar population, while in starbursts we observe a significant amount of underlying old stellar population, which contributes mostly to the visual and near-IR parts of the SED.

The comparison between the SEDs of SNRs and starbursts shows that non-thermal SNRs and starbursts are similar only in the radio, with the non-thermal SNR being stronger in X-rays and fainter in the other wavebands. The thermal SNR and the starbursts have similar SEDs in the radio. Thermal SNRs are fainter than Starbursts in the visual to mid/far-IR, but fainter in the UV and X-rays.

7. ARE THE DIFFERENT ACTIVITY CLASSES DISTINGUISHABLE BY THEIR SEDs?

Can we distinguish between different classes of galaxies based on their SEDs? In order to statistically study this we have chosen several wavebands, normalized to the λ7000 Å flux, and compared the different SEDs using student's t-test. We use here the normalization to the λ7000 Å flux because it represents a normalization to the old stellar population. However, it should be kept in mind that a different normalization would produce different results, such as with the normalization of LINER's and Seyfert 2's at 60 μm. Table 8 shows the wavebands used and the number of galaxies with those wavebands available in each group. The results of the comparison are shown in Table 9 and Fig. 10, where we give the probability of two SEDs being equal. Two SEDs are considered to be significantly different when the t-test gives probabilities smaller than 0.05 (5%), which corresponds to 2σ difference. This value is noted with a line in Fig. 10. If the probability is between 0.05 and 0.2 (between ≈1.3 and 2.0 σ), the SEDs are considered to be moderately different, which means that this difference can be considered as a tendency, but should be used with caution to distinguish between two different activity classes. Notice that we are not comparing the 6 cm and X-ray emission of normal Spirals with other galaxies, because there is only a small number of Spirals detected in these wavebands.

On the bottom panel of Fig. 10 we compare objects of similar activity class. In agreement with the results of the previous section, SBH's and SBL's can be well distinguished in the visual UV and far-IR parts of the spectrum. Seyfert 2 and LINER SEDs are significantly different only at 25 μm. However, with the exception of the near-IR optical band (14<log ν<14.5 Hz), where they are very similar, the probability of the two SEDs being equal, in the remaining wavebands, is only moderately significant. The comparison between Ellipticals and Spirals shows that their SEDs are very similar. Only in the UV (1355 Å) the probability of the two distributions being equal reaches values smaller than 0.15.

On the middle panel we compare active (Seyfert 2, LINER, SBH, and SBL) with normal spiral galaxies SEDs. We chose to compare the active galaxies only to the normal spirals, because the ellipticals SEDs are very similar to them, and also because the host galaxies of the active objects are spirals. The spirals can be separated from SBH's and SBL's in the mid/far-IR, visual and UV wavebands. The comparison with the Seyfert 2 template shows that the two SEDs can be well separated in the mid/far-IR and also in the UV (2900 Å). LINER's and spirals are similar along most of the energy spectrum. Only in the mid/far-IR is the probability of the two distributions close enough to 0.05 for them to be considered as moderately different.

On the top panel of Fig. 10 we compare the SEDs of SBH's and SBL's with Seyfert 2's and LINER's. Seyfert 2's SED is different from both SBH's and SBL's in the visual and UV waveband, and also different from SBL's in the near-IR. It can be considered as moderately different from SBH's in the X-rays and near-IR. The LINER's SED is different, or moderately different from that of SBLs in the UV

TABLE 9. Probability of two SEDs being equal.

Ratios	$E\times$Sp	Sy2×LIN	SBL×SBH	Sy2×SBH	Sy2×SBL	LIN×SBH	LIN×SBL	SBH×Sp	SBL×Sp	Sy2×Sp	LIN×Sp
Log (6 cm/7000 Å)	—	0.173	0.927	0.720	0.645	0.250	0.259	—	—	—	—
Log (100 μm/7000 Å)	0.641	0.084	0.041	0.257	0.185	0.036	0.188	0.005	0.014	0.009	0.067
Log (25 μm/7000 Å)	0.962	0.043	0.694	0.565	0.317	0.058	0.071	0.000	0.000	0.000	0.065
Log (2.2 μm/7000 Å)	0.485	0.249	0.115	0.066	0.001	0.427	0.029	0.413	0.201	0.976	0.612
Log (1.6 μm/7000 Å)	0.724	0.769	0.267	0.084	0.007	0.258	0.065	0.483	0.305	0.957	0.853
Log (1.2 μm/7000 Å)	0.797	0.962	0.285	0.204	0.017	0.311	0.069	0.396	0.221	0.748	0.738
Log (5310 Å/7000 Å)	0.971	0.089	0.000	0.070	0.000	0.011	0.000	0.017	0.000	0.263	0.397
Log (2900 Å/7000 Å)	0.246	0.157	0.005	0.003	0.000	0.031	0.006	0.004	0.000	0.048	0.950
Log (2530 Å/7000 Å)	0.888	0.134	0.004	0.001	0.000	0.032	0.008	0.012	0.003	0.046	0.495
Log (1507 Å/7000 Å)	0.264	0.129	0.000	0.000	0.000	0.036	0.013	0.162	0.075	0.446	0.590
Log (1355 Å/7000 Å)	0.126	0.109	0.000	0.000	0.000	0.033	0.011	0.048	0.013	0.233	0.519
Log (X-rays/7000 Å)	—	0.082	0.951	0.137	0.370	0.493	0.758	—	—	—	—

to mid IR range. When compared to SBH's, LINER's are different in the UV, visual and mid/far IR wavebands.

In conclusion, the statistical analysis confirms the qualitative results from the previous sections. The largest differences over the entire 10 decades of frequency exist between LINER's and SBL's. In all other cases, the differences are limited to specific ranges, such as those between Seyfert 2's and LINER's in the mid/far-IR and UV. Normal galaxies can be separated from active ones (Starbursts, LINER's and Seyfert 2's) by the lower mid/far-IR, and UV emission, relative to the visual. Seyfert 2's and LINER's can be easily differentiated from Starbursts, based on their smaller UV/visual ratio.

8. BOLOMETRIC FLUXES

The bolometric fluxes were calculated by integrating the SEDs. The contribution of the X-ray band to the bolometric luminosity is very small, and consequently does not affect the results for those galaxies without data available in this waveband. A comparison between the bolometric fluxes and galaxy diameters shows that these quantities are independent. This result assures us that the flux of wavebands like the mid/far-IR, which were observed through apertures much larger than that of the *IUE*, are not shifting the bolometric flux of large objects to higher values.

In Fig. 11 we compare the bolometric flux with the flux density of selected wavebands. Considering all galaxies together, the 100 μm flux density shows the best correlation with the bolometric flux. When we consider only galaxies of the same activity class, their bolometric fluxes also show a good correlation with the flux density in other wavebands. We can also see in this figure that the wavebands which contribute most to the bolometric flux in Seyfert 2's, LINER's, and Starbursts are the mid/far-IR. For normal galaxies, the emission from these wavebands is weaker and the wavebands which contribute most to the bolometric flux are the near-IR and visual.

The observed correlation can be used to obtain the bolometric flux of galaxies with different activity classes, based on information of a limited wavelength range. In order to quantify this, we separate the galaxies in groups, according to activity class: Normal galaxies (Spirals+Ellipticals), Seyfert 2's, SBL's, and SBH's. LINER's are excluded from this analysis because of the small number of objects in the sample. For these groups we perform linear fits of the form $\log(F_{\rm bol}) = a + b \times \log(\nu F_\nu)$.

The resulting coefficients "a" and "b," as well as the correlation coefficients of the linear fits are given in Table 10. For normal galaxies, the near-IR wavebands are the ones which better correlate with the bolometric flux. For Seyfert 2's the bolometric flux correlates well with the flux in the mid/far-IR bands. SBL's bolometric flux correlates well with the fluxes of the wavebands in the range 2530 Å to far-IR, while for SBH's the best correlation is in near and far-IR.

9. SUMMARY

In this paper we built the radio to X-ray SEDs of 59 galaxies, including normal spirals, ellipticals, LINER's, Seyfert 2's, and starbursts. Also, for the comparison with starbursts, we built SEDs for H II regions, thermal and nonthermal SNRs. We used data selected from the literature,

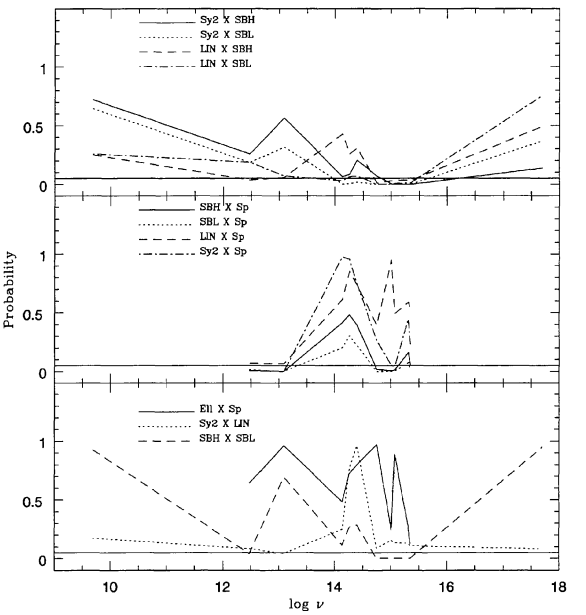

FIG. 10. Probability of two SEDs being equal as a function of the waveband. The horizontal line at 0.05 represents the probability below which two SEDs can be considered different. When the probability is between 0.05 and 0.2 the SEDs are moderately different.

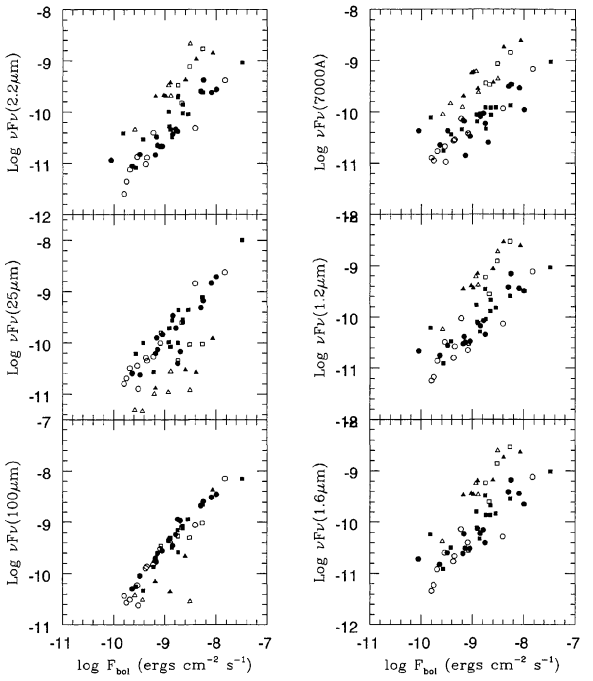

FIG. 11. Relations between Bolometric flux and the flux densities at six wavebands, 100 μm (left bottom), 25 μm (left middle), 2.2 μm (left top), 1.6 μm (right bottom), 1.2 μm (right middle), and 7000 Å (right top). The vertical axis has units of ergs cm^{-2} s^{-1}. Filled squares represent Seyfert 2's, open squares LINER's, filled triangles normal ellipticals, open triangles normal spirals, filled circles SBH's and open circles represent SBL's.

trying to match the *IUE* aperture ($10'' \times 20''$), and discuss the possible contamination effects for the wavebands observed with larger apertures.

The SEDs were normalized to the flux at λ7000 Å, which corresponds to a normalization by the old stellar population, and averaged according to their activity and morphological classes. Both a qualitative and a quantitative comparison between the SEDs of different classes of objects were performed, giving similar results, which can be summarized as follows. The normal spirals and ellipticals have similar SEDs over the entire energy range, but are fainter than the other SEDs, relative to the λ7000 Å flux. The Seyfert 2 SEDs are similar to those of LINER's in the visual and near-IR, but stronger in the other wavebands. When compared to Starbursts, Seyfert 2's have similar SEDs in the radio to near-IR, are weaker in the ultraviolet, but stronger in the X-rays. The SBH's and SBL's SED's are very similar along the entire energy range, with the exception of the ultraviolet, where SBH's are weaker, and mid/far-IR, where they are stronger. These differences can be accounted to the higher absorption and reradiation of the ionizing radiation in SBH's.

The SEDs of Seyfert 2's, LINER's, and starbursts were compared with SEDs of RQQ and RLQ, normalized to the flux at λ60 μm. The quasars SEDs are between 1 and 2 dex stronger than the other SEDs, depending on the waveband. The exception occurs for RQQ SEDs, which are similar to those of the other galaxies in the radio to far-IR wavebands. From this comparison we have also found that, when using the normalization at λ60 μm, the SEDs of LINER's and Seyfert 2's are very similar, with the exception of the optical to near-IR wavebands where LINER's are dominated by the old stellar population.

We have also constructed SEDs of H II regions, thermal and non-thermal SNRs. H II regions and thermal SNRs have similar SEDs and differ only in the X-rays, where H II regions are fainter, and far-IR, where H II regions are stronger. The SED of the non-thermal SNR is a flat continuum, for which we do not have a good normalization point to compare with the other SEDs. The comparison of starbursts with H II regions shows that they are very similar, with the exception of the X-rays, visual and near-IR, where starbursts are stronger, due to the contribution from old stars in the visual and near-IR, and "superwinds" in X-rays (Heckman *et al.* 1990).

Finally, we calculated the bolometric fluxes of the galaxies and compared them with the flux densities of individual wavebands. From this comparison we found that the mid/far-IR emission dominates the energy output in Seyfert 2's, LINER's, and Starbursts. For spirals and ellipticals the visual and near-IR emission contributes most to the bolometric flux. We have also performed linear regressions between the bolometric fluxes and flux densities, which can be used to de-

TABLE 10. Linear regression coeficients between log(F_{Bol}) and log(νF_ν).

	Normals			Seyfert 2's			SBL's			SBH's		
νF_ν	*a*	*b*	*r*	*a*	*b*	*r*	*a*	*b*	*r*	*a*	*b*	*r*
6 cm	−4.48	1.09	0.33	−6.35	0.95	0.63	−6.92	0.90	0.79	−13.22	0.19	0.22
100 μm	−0.91	1.04	0.53	0.32	1.10	0.96	1.26	1.21	0.97	0.80	1.14	0.98
25 μm	−4.04	0.76	0.87	0.10	1.11	0.91	0.86	1.19	0.97	−0.33	1.07	0.89
2.2 μm	−0.16	1.05	0.92	−3.41	0.76	0.86	−2.16	0.93	0.94	−2.53	0.88	0.93
1.6 μm	0.67	1.13	0.93	−3.67	0.71	0.85	−2.14	0.91	0.91	−3.12	0.79	0.89
1.2 μm	0.56	1.11	0.95	−3.92	0.68	0.84	−2.28	0.89	0.90	−3.00	0.80	0.91
7000 Å	−1.64	0.88	0.87	−5.07	0.57	0.84	−2.58	0.85	0.96	−5.72	0.50	0.70
5310 Å	−1.75	0.88	0.86	−5.31	0.55	0.82	−2.63	0.85	0.97	−5.93	0.49	0.71
2900 Å	−5.74	0.56	0.67	−7.18	0.42	0.62	−3.48	0.76	0.94	−7.68	0.32	0.65
2530 Å	−4.73	0.74	0.47	−7.25	0.43	0.57	−3.55	0.75	0.93	−7.95	0.29	0.61
1507 Å	−13.10	−0.21	0.29	−7.75	0.38	0.48	−4.28	0.67	0.85	−9.27	0.16	0.40
1355 Å	−11.93	−0.06	0.06	−8.26	0.34	0.36	−4.18	0.68	0.82	−9.23	0.17	0.39
X-ray	−21.32	−1.09	0.78	−7.41	0.55	0.53	−9.99	0.28	0.32	−7.40	0.59	0.69

termine the bolometric flux of objects with reduced waveband information.

This work was supported by NASA under Grant No. NAGW-3757 and by the Brazilian institution CNPq. This research has made use of the NASA/IPAC Extragalactic Database (NED) which is operated by the Jet Propulsion Lab, Caltech, under contract with NASA. We would like to thank N. Panagia and K. Long for useful discussions about supernova remnants.

REFERENCES

Aaronson, M. 1977, Ph.D. dissertation, Harvard University
Allen, D. A. 1976, ApJ, 207, 367
Alloin, D., *et al.* 1995, A&A, 293, 293
Antonucci, R., Barvainis, R., & Alloin, D. 1990, ApJ, 353, 416
Artyukh, V. S., & Ogannisyam, M. A. 1983, Afz, 19, 655
Balzano, V. A., & Weedman, D. W. 1981, ApJ, 243, 756
Bartel, N., *et al.* 1982, ApJ, 262, 556
Batuski, D. J., Hanisch, R. J., & Burns, J. O. 1992, AJ, 103, 1077
Baum, S. A., O'Dea, C. P., Dallacassa, D., DeBruyn, A. G., & Pedlar, A. 1993, ApJ, 419, 553
Biermann, P., Clarke, J. N., Fricke, K. J., Pauliny-Toth, I. I. K., Schmidt, J., & Witzel, A. 1980, A&A, 81, 235
Blitz, L., Israel, F. P., Neugebauer, G., Gatley, I., Lee, T. J., & Beattie, D. H. 1981, ApJ, 249, 76
Boller, Th., Meurs, E. J. A., Brinkmann, W., Fink, H., Zimmermann, U., & Adorf, H. M. 1992, A&A, 261, 57
Buczilowski, U. R. 1988, A&A, 205, 29
Calzetti, D. 1997, AJ, 113, 162
Calzetti, D., Kinney, A. L., & Storchi-Bergmann, T. 1994, ApJ, 429, 582
Calzetti, D., Bohlin, R. C., Kinney, A. L., Storchi-Bergmann, T., & Heckman, T. M. 1995, ApJ, 443, 136
Campbell, A. W., & Terlevich, R. 1984, MNRAS, 211, 15
Cameron, M. J. 1971, MNRAS, 152, 403
Condon, J. J. 1980, ApJ, 242, 894
Condon, J. J. 1983, ApJS, 53, 459
Condon, J. J. 1987, ApJS, 65, 485
Condon, J. J., & Broderick, J. J. 1988, AJ, 96, 30
Condon, J. J., & Broderick, J. J. 1991, AJ, 102, 1663
Condon, J. J., Frayer, D. T., & Broderick, J. J. 1991, AJ, 101, 362
Condon, J. J., Helou, G., Sanders, D. B., & Soifer, B. T. 1990, ApJS, 73, 359
Condon, J. J., & Jaucey, D. L. 1974, AJ, 79, 437
Cox, M. J., Eales, S. A. E., Alexander, P., & Fitt, A. J. 1988, MNRAS, 235, 1227
Deeg, H.-J., Brinks, E., Duric, N., Klein, U., & Skillman, E. 1993, ApJ, 410, 626
Dennison, B., Balonek, T. J., Terzian, Y., & Balick, B. 1975, PASP, 87, 83
deVaucoulers, A., & Longo, G. 1988, Catalogue of Visual and Infrared Photometry of Galaxies from 0.5 microns to 10 microns (1961–1985), University of Texas at Austin
D'Odorico, S., Rosa, M., & Wampler, E. J. 1983, A&AS, 53, 97
Dressel, L. L., & Condon, J. J. 1978, ApJS, 36, 53
Dyck, H. M., Becklin, E. E., & Capps, R. W. 1978, BAAS, 10, 422
Edelson, R. A., & Malkan, M. A. 1986, ApJ, 308, 59
Ellis, R. S., Gondhalekar, P. M., & Efstathiou, G. 1982, MNRAS, 201, 223
Fabbiano, G. 1989, ARA&A, 27, 87
Fabbiano, G., Kim, D.-W., & Trinchieri, 1992, ApJS, 80, 531
Ficarra, A., Grueff, G., & Tomassetti, G. 1985, A&AS, 59, 255
Fitzpatrick, E. L. 1986, AJ, 92, 1068
Forbes, D. A., & Ward, M. J. 1993, ApJ, 416, 150
Frogel, J. F., Elias, J. H., & Phillips, M. M. 1982, ApJ, 260, 70
Frogel, J. A., Persson, S. E., Aaronson, M., & Matthews, K. 1978, ApJ, 220, 75
Gallagher, J. S., Goad, J. W., & Mould, J. 1982, ApJ, 263, 101
Garnett, D. R. 1989, ApJ, 345, 282
Genzel, R., Pauliny-Toth, I. I. K., Preuss, E., & Witzel, A. 1976, AJ, 81, 1084
Glass, I. S. 1973, MNRAS, 164, 155
Glass, I. S. 1976, MNRAS, 175, 191
Glass, I. S. 1978, MNRAS, 183, 85
Glass, I. S. 1979, MNRAS, 186, 29
Glass, I. S. 1981, MNRAS, 197, 1067
Glass, I. S. 1984, MNRAS, 211, 461
Glass, I. S., & Moorwood, A. F. M. 1985, MNRAS, 214, 429
Goudfrooij, P., & de Jong, T. 1995, A&A, 298, 784
Gregory, P. C., & Condon, J. J. 1991, ApJS, 75, 1011
Griersmith, D., Hyland, A. R., & Jones, T. J. 1982, AJ, 87, 1106
Harnett, J. I. 1982, AuJPh, 35, 321
Harnett, J. I. 1984, MNRAS, 210, 13
Harnett, J. I. 1987, MNRAS, 227, 887
Heckman, T. M., Armus, L., & Miley, G. K. 1990, ApJS, 74, 833
Heidmann, J., Klein, U., & Wielibinski, R. 1982, A&A, 105, 188
Hummel, E. 1980, A&AS, 41, 151
Hummel, E., van der Hulst, J. M., & Dickey, J. M. 1984, A&A, 134, 207
Hunter, D. A., & Gallagher, III, J. S. 1985, AJ, 90, 1457
Israel, F. P., & Mahoney, M. J. 1990, ApJ, 352, 30
Israel, F. P., Mahoney, M. J., & Howarth, N. 1992, A&A, 261, 47
Israel, F. P., & van der Hulst, J. M. 1983, AJ, 88, 1736
Joyce, R. R., & Simon, M. 1976, PASP, 88, 870
Kellerman, K. I., Pauliny-Toth, I. I. K., & Williams, P. J. S. 1969, ApJ, 157, 1
Kinney, A. L., Bohlin, R. C., Calzetti, D., Panagia, N., & Wyse, R. F. G. 1993, ApJS, 86, 5
Kinney, A. L., Calzetti, D., Bohlin, R. C., McQuade, K., Storchi-Bergmann, T., & Schmitt, H. R. 1996, ApJ, 467, 38
Klein, U., Gräve, R., & Wielebinski, R. 1983, A&A, 117, 332
Klein, U., & Gräve, R. 1986, A&A, 161, 155
Klein, U., Weiland, H., & Brinks, E. 1991, A&A, 246, 323
Klein, U., Wielebinski, R., & Thuan, T. X. 1984, A&A, 141, 241
Kleinmann, D. E., & Wright, E. L. 1974, ApJ, 191, L19
Knapp, G. R., Guhathakurta, P., Kim, D.-W., & Jura, M. 1989, ApJS, 70, 329
Kojoian, G., Tovmassian, H. M., Dickinson, D. F., & Dinger, A. S. C. 1980, AJ, 85, 1462
Kollatschny, W., Biermann, R., Friecke, K. J., Huchtmeier, W., & Witzel, A. 1983, A&A, 119, 80
Kühr, H., Witzel, A., Pauliny-Toth, & Nauber, U. 1981, A&AS, 45, 367
Lawrence, A., Rowan-Robinson, M., Efstathiou, A., Ward, M. J., Elvis, M., Smith, M. G., Duncan, W. D., & Robson, E. I. 1991, MNRAS, 248, 91
Lebofski, M. J., & Rieke, G. H. 1979, ApJ, 229, 111
Longmore, A. J., & Sharples, R. M. 1982, MNRAS, 201, 111
Mas-Hesse, J. M., Rodríguez-Pascual, P. M., de Córdoba, L. S. F., & Mirabel, I. F. 1994, ApJS, 92, 599
Mas-Hesse, J. M., Rodríguez-Pascual, P. M., de Córdoba, L. S. F., Mirabel, I. F., Wamsteker, W., Makino, F., & Otani, C. 1995, A&A, 298, 22
McAlary, C. W., McLaren, R. A., & Crabtree, D. R. 1979, ApJ, 234, 471
McQuade, K., Calzetti, D., & Kinney, A. L. 1995, ApJS, 97, 331
Meurs, E. J., & Wilson, A. S. 1984, A&A, 136, 206
Moorwood, A. F. M., & Glass, I. S. 1982, A&A, 115, 84
Morris, S., Ward, M., Whittle, M., Wilson, A. S., & Taylor, K. 1985, MNRAS, 216, 193
Oly, C., & Israel, F. P. 1993, A&AS, 100, 263
Ondrechen, M. P. 1985, AJ, 90, 1474
Pauliny-Toth, I. I. K., Witzel, A., Preuss, E., Kühr, H., Kellermann, K. I., Fomalont, E. B., & Davis, M. M. 1978, AJ, 83, 451
Penston, M. V. 1973, MNRAS, 162, 359
Persson, S. E., Cohen, J. G., Sellgren, K., Mould, J., & Frogel, J. A. 1980, ApJ, 240, 779
Persson, S. E., Frogel, J. A., & Aaronson, M. 1979, ApJS, 39, 61
Pier, E. A., & Krolik, J. H. 1992, ApJ, 401, 99

Pilkington, J. D. H., & Scott, P. F. 1965, MemRAS, 69, 183
Rieke, G. H. 1978, ApJ, 226, 550
Rieke, G. H., & Lebofsky, M. J. 1978, ApJ, 220, L37
Rieke, G. H., & Low, F. J. 1972, ApJ, 176, L95
Rosa, M., Joubert, M., & Benvenutti, P. 1984, A&AS, 57, 361
Rudy, R. J., LeVan, P. D., & Rodriguez-Espinosa, J. M. 1982, AJ, 87, 598
Sadler, E. M. 1984, AJ, 89, 53
Sadler, E. M., Jenkins, C. R., & Kotanyi, C. G. 1989, MNRAS, 240, 591
Sanamyan, V. A., Kandalyan, R. A., & Oganyan, G. A. 1983, Afz, 19, 429
Sandage, A. R., Becklin, E. E., & Neugebauer, G. 1969, ApJ, 157, 55
Sanders, D. B., Phinney, E. S., Neugebauer, G., Soifer, B. T., & Matthews, K. 1989, ApJ, 347, 29
Schommer, R. A., Caldwell, N., Wilson, A. S., Baldwin, J. A., Phillips, M. M., Willians, T. B., & Turtle, A. J. 1988, ApJ, 324, 154
Schulman, E., & Bregman, J. N. 1995, ApJ, 441, 568
Schwering, P. B. W., & Israel, F. P. 1990, Atlas and Catalogue of IR Sources in the Magellanic Clouds (Kluwer, Dordrecht)
Skilman, E. D., & Klein, U. 1988, A&A, 199, 61
Slee, O. B., & Higgins, C. S. 1973, AuJPA, 27, 1
Spinoglio, L., Malkan, M. A., Rush, B., Carrasco, L., & Recillas-Cruz, E. 1995, ApJ, 453, 616
Sramek, R. A., & Weedman, D. W. 1986, ApJ, 302, 640
Storchi-Bergmann, T., Kinney, A. L., & Challis, P. 1995, ApJS, 98, 103
Storchi-Bergmann, T., Mulchaey, J. S., & Wilson, A. S. 1992, ApJ, 395, L73
Stothers, R., & Chin, C.-W. 1972, ApJ, 177, 155
Stull, M. A. 1971, AJ, 76, 1
Subrahmanya, C. R., & Harnett, J. I. 1987, MNRAS, 225, 297
Telesco, C. M., & Gatley, I. 1981, ApJ, 247, L11
Thronson, Jr., H. A., Walker, C. K., Walker, C. E., & Maloney, P. 1987, ApJ, 318, 645
Thuan, T. X. 1983, ApJ, 268, 667
Torres-Peimbert, S., Peimbert, M., & Fierro, J. 1989, ApJ, 345, 186
Tovmassian, H. M., Sherwood, W. A., Sherwood, V. E., Schultz, G. V., Salter, C. J., & Matthews, H. E. 1984, A&AS, 58, 317
Tovmassian, H. M., & Terzian, Y. 1974, PASP, 86, 649
Ulvestad, J. S., & Wilson, A. S. 1984a, ApJ, 278, 544
Ulvestad, J. S., & Wilson, A. S. 1984b, ApJ, 285, 439
Ulvestad, J. S., & Wilson, A. S. 1989, ApJ, 343, 659
Unger, S. W., Pedlar, A., Booler, R. V., & Harrison, B. A. 1986, MNRAS, 219, 387
Vancura, O., Blair, W. P., Long, K. S., & Raymond, J. C. 1992, ApJ, 394, 158
van Driel, W., van den Broek, A. C., & de Jong, T. 1991, A&AS, 90, 55
Vila, M. B., Pedlar, A., Davies, R. D., Hummel, E., & Axon, D. J. 1990, MNRAS, 242, 379
Ward, M., Penston, M. V., Blades, J. C., & Turtle, A. J. 1980, MNRAS, 193, 563
Ward, M., Allen, D. A., Wilson, A. S., Smith, M. G., & Wright, A. E. 1982, MNRAS, 199, 953
Williams, R. M., & Chu, Y.-H. 1995, ApJ, 439, 132
Wills, B. J. 1975, AuJPA, 38, 1
Woltjer, L. 1987, in High Energy Phenomena Around Collapsed Stars, edited by Pacini (Holland, Dordrecht), p. 209
Wright, A. E. 1974, MNRAS, 167, 273
Wright, A., & Otrupcek, R. 1990, PKSCAT90, the Southern Radio Source Database, Australian Telescope National Facility
Wynn-Williams, C. G., & Becklin, E. E. 1986, ApJ, 308, 620